EUROPEAN ORGANIZATION FOR NUCLEAR RESEARCH (CERN)

CERN-EP-2024-025
2024/05/21

CMS-EXO-23-014

Search for long-lived particles decaying to final states with a pair of muons in proton-proton collisions at $\sqrt{s} = 13.6\,\text{TeV}$

The CMS Collaboration*

Abstract

An inclusive search for long-lived exotic particles (LLPs) decaying to final states with a pair of muons is presented. The search uses data corresponding to an integrated luminosity of 36.6 fb^{-1} collected by the CMS experiment from the proton-proton collisions at $\sqrt{s} = 13.6\,\text{TeV}$ in 2022, the first year of Run 3 of the CERN LHC. The experimental signature is a pair of oppositely charged muons originating from a secondary vertex spatially separated from the proton-proton interaction point by distances ranging from several hundred μm to several meters. The sensitivity of the search benefits from new triggers for displaced dimuons developed for Run 3. The results are interpreted in the framework of the hidden Abelian Higgs model, in which the Higgs boson decays to a pair of long-lived dark photons, and of an R-parity violating supersymmetry model, in which long-lived neutralinos decay to a pair of muons and a neutrino. The limits set on these models are the most stringent to date in wide regions of lifetimes for LLPs with masses larger than 10 GeV.

Published in the Journal of High Energy Physics as doi:10.1007/JHEP05(2024)047.

*See Appendix A for the list of collaboration members

1 Introduction

Long-lived particles (LLPs) that are unobserved as yet are predicted by many extensions of the standard model (SM), in particular by various supersymmetry (SUSY) scenarios [1, 2] and "hidden-sector" models [3, 4]. Such particles could manifest themselves through decays to SM particles at macroscopic distances from the proton-proton (pp) interaction point (IP).

This paper describes an inclusive search for an exotic massive LLP decaying to a pair of oppositely charged muons, referred to as a "displaced dimuon", originating from a secondary vertex spatially separated from the IP. The analysis is based on a data set of pp collisions corresponding to an integrated luminosity of 36.6 fb^{-1} collected with the CMS detector at $\sqrt{s} = 13.6\,\text{TeV}$ during 2022, the first year of Run 3 of the CERN LHC. It is a continuation and extension of the CMS analysis [5] performed using data collected at $\sqrt{s} = 13\,\text{TeV}$ during Run 2 (2016–2018) and corresponding to an integrated luminosity of 97.6 fb^{-1} (referred to below as the CMS Run 2 analysis). A minimal set of requirements and loose event selection criteria allow the search to be sensitive to a wide range of models predicting LLPs that decay to final states that include a pair of oppositely charged muons. Improvements in the triggers result in a significantly higher efficiency for displaced dimuons in Run 3, particularly at dimuon masses of a few tens of GeV. The present search explores the LLP mass range above 10 GeV and is sensitive to vertex displacements ranging from several hundred μm to several meters.

We interpret the results of the search in the frameworks of two benchmark models: the hidden Abelian Higgs model (HAHM), in which displaced dimuons arise from decays of hypothetical dark photons [6], and a simplified SUSY model, in which long-lived neutralinos decay to a pair of muons and a neutrino as a result of R-parity violation (RPV) [2]. The results for the HAHM model from Run 3 are statistically combined with the results of the Run 2 analysis [5]. The Run 2 search [5] and the present search are complementary to a CMS search [7], which uses data collected in Run 2 with a dedicated high-rate data stream in order to explore otherwise inaccessible parameter space at low dimuon masses. A search for LLPs decaying to displaced dimuons has also been performed by CMS in Run 1, using data taken at $\sqrt{s} = 8\,\text{TeV}$ and corresponding to an integrated luminosity of 20.5 fb^{-1} [8, 9], and by the ATLAS Collaboration in Run 2, using data corresponding to an integrated luminosity of 32.9 fb^{-1} [10, 11].

This paper is organized as follows. Section 2 describes the CMS detector. Section 3 presents the signal models, as well as the simulated signal and background event samples. Section 4 describes the analysis strategy, the triggers, and the offline event selection. Estimation of backgrounds and the associated systematic uncertainties are described in Section 5. Section 6 summarizes the systematic uncertainties affecting signal efficiencies. Section 7 describes the results of this analysis and their combination with the results of the CMS Run 2 analysis. The summary of the paper is given in Section 8. Tabulated results and supplementary material for reinterpreting the results in the framework of models not explicitly considered in this paper are provided in the HEPData record for this analysis [12].

2 The CMS detector

The central feature of the CMS detector is a superconducting solenoid of 6 m internal diameter, providing a magnetic field of 3.8 T. Within the solenoid volume are a silicon pixel and strip tracker extending outwards to a radius of 1.1 m, a lead tungstate crystal electromagnetic calorimeter, and a brass and scintillator hadron calorimeter, each composed of a barrel and two endcap sections. Forward calorimeters extend the coverage in pseudorapidity η provided by the barrel and endcap detectors. Muons are detected in gas-ionization chambers covering the

range $|\eta| < 2.4$ and embedded in the steel flux-return yoke outside the solenoid. The muon system is composed of four types of chambers: drift tubes (DTs) in the barrel ($|\eta| < 1.2$), cathode strip chambers (CSCs) in the endcaps ($0.9 < |\eta| < 2.4$), resistive-plate chambers in both the barrel and the endcaps, and gas electron multipliers in the forward regions of the endcaps. The chambers are assembled into four "stations" at increasing distance from the IP. The stations in the barrel are located approximately 4, 5, 6, and 7 m away from the IP radially, while the stations in the endcap are located approximately 7.0, 8.0, 9.5, and 10.5 m away from the IP along the beam line axis on both ends of the detector. Each station provides reconstructed hits in several detection planes, which are combined into track segments, forming the basis of muon reconstruction in the muon system [13]. A more detailed description of the CMS detector, together with a definition of the coordinate system used and the relevant kinematical variables, can be found in Refs. [14, 15].

Events of interest are selected using a two-tiered trigger system. The first level (L1), composed of custom hardware processors, uses information from the calorimeters and muon detectors to select events at a rate of approximately 100 kHz within a fixed latency of 4 μs [16]. At the next stage, a farm of processors running a version of the full event reconstruction software optimized for fast processing, known as the high-level trigger (HLT), reduces the event rate to about 1 kHz before data storage [17]. At the HLT, muon candidates are reconstructed in two steps. In the first step, referred to as Level 2 (L2), muons are reconstructed using only the information from the muon detectors, whereas at the stage referred to as Level 3 (L3), tracker information is also used.

3 Signal models and simulated samples

Two signal models with different final-state topologies and event kinematics are used in the optimization of event selection criteria and in the interpretation of results. The first belongs to a class of models featuring a "hidden" or "dark" sector of matter that does not interact directly with the SM particles, but can manifest itself through mixing effects. This HAHM benchmark [6, 18] contains an extra dark gauge field $U(1)_D$, which mixes kinetically with the hypercharge SM gauge field ("vector portal") and gives rise to a spin-1 mediator known as the dark photon Z_D. The symmetry of $U(1)_D$ is broken by a new dark Higgs field H_D, which mixes with the SM Higgs boson H ("Higgs portal") and gives mass $m(Z_D)$ to the dark photon. If there are no hidden-sector states with masses smaller than $m(Z_D)$, the mixing through the vector portal with the SM photon and Z boson causes the dark photon to decay exclusively to SM particles, with a sizable branching fraction to leptons. Pair production of the Z_D via the Higgs portal with subsequent decays of dark photons via the vector portal is shown in Fig. 1 (left).

The present search probes the regime of $m(Z_D) > 10$ GeV with small values of the Z–Z_D kinetic mixing parameter ϵ [6]. In this regime, the dark photon is long-lived, since its mean proper lifetime $\tau(Z_D)$ is proportional to ϵ^{-2}. In particular, the dark photon with $10\,\text{GeV} \lesssim m(Z_D) < m(H)/2$ is expected to have macroscopically large mean proper decay lengths, for example, $c\tau(Z_D) \gtrsim \mathcal{O}(100\,\mu\text{m})$ for $\epsilon < \mathcal{O}(10^{-6})$. The Z_D production rate is governed by the branching fraction $\mathcal{B}(H \to Z_D Z_D)$, which does not depend on ϵ but is proportional to the square of $\kappa m^2(H)/|m^2(H) - m^2(H_D)|$, where κ is the H–H_D mixing parameter. Since κ and $m(H_D)$ affect only the overall dark photon production rate, sampling of $m(Z_D)$ and ϵ is sufficient to explore different kinematical and topological scenarios of the model. We generated a set of 24 simulated HAHM event samples with $m(Z_D)$ between 10 and 60 GeV and ϵ between 10^{-7} and 2×10^{-9}. In this mass range, the model's prediction for $\mathcal{B}(Z_D \to \mu^+\mu^-)$ varies between 15.4% at $m(Z_D) =$

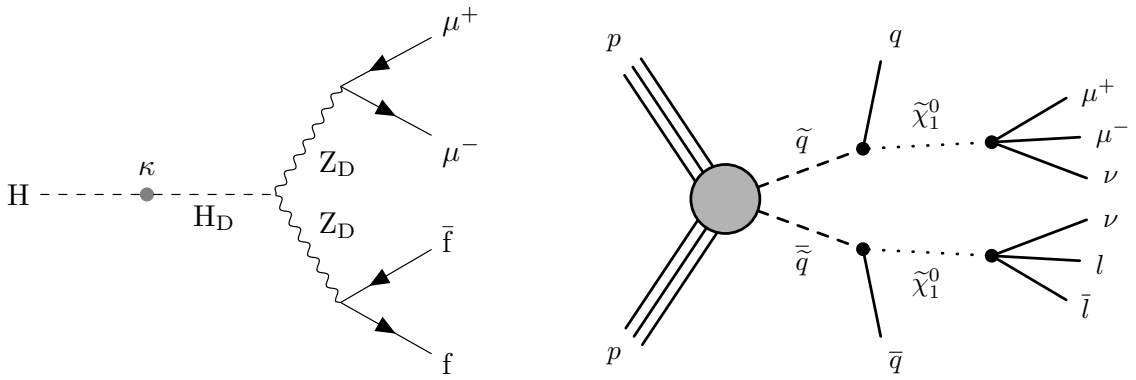

Figure 1: Feynman diagrams for (left) the HAHM model, showing the production of long-lived dark photons Z_D via the Higgs portal, through H–H_D mixing with the parameter κ, with subsequent decays to pairs of muons or other fermions via the vector portal; and (right) pair production of squarks followed by $\tilde{q} \to q\tilde{\chi}_1^0$ decays, where the RPV neutralino is assumed to be a long-lived particle that decays into a neutrino and two charged leptons.

10 GeV and 10.7% at $m(Z_D) = 60$ GeV. The dark Higgs boson is assumed to be heavy enough so that $H \to H_D H_D$ decays are kinematically forbidden. (In the sample generation, we use $m(H_D) = 400$ GeV and $\kappa = 0.01$.) The production of dark photons is modeled at leading order by MADGRAPH5_aMC@NLO [19] version 2.9.9. The samples are generated only for the dominant gluon-fusion production mechanism, but the Higgs boson production cross section is normalized to the most recent theoretical prediction for the sum of all production modes for $m(H) = 125$ GeV at $\sqrt{s} = 13.6$ TeV, 59.8 pb [20, 21]. The decays of the dark photons are modeled by PYTHIA 8.306 [22].

We also consider a simplified benchmark model inspired by RPV SUSY and featuring displaced $\mu^+\mu^-\nu$ vertices. Unlike the HAHM, where the two-body LLP decay leads to displaced $\mu^+\mu^-$ vertices that are reconstructed with the dimuon invariant mass $m_{\mu\mu}$ corresponding to the LLP mass, the presence of a neutrino at the decay vertex leads to a nonpeaking $m_{\mu\mu}$ distribution with a broad spectrum below the endpoint at the LLP mass. In this model, which was used by CMS in the Run 1 searches for displaced dimuons [8, 9] and by ATLAS in the Run 2 search for pairs of displaced charged leptons [11], the LLP is assumed to be an RPV neutralino $\tilde{\chi}_1^0$ that results from decays of mass-degenerate squarks, $\tilde{q} \to q\tilde{\chi}_1^0$, which are pair produced in pp collisions. Nonzero values of RPV couplings λ_{122} and λ_{232} enable displaced $\tilde{\chi}_1^0$ decays into a pair of oppositely charged muons and a neutrino, $\tilde{\chi}_1^0 \to \mu^+\mu^-\nu$ [23, 24]. The Feynman diagram for this process is shown in Fig. 1 (right).

The search uses benchmark signal samples that are generated assuming $\mathcal{B}(\tilde{\chi}_1^0 \to \mu^+\mu^-\nu) = \mathcal{B}(\tilde{\chi}_1^0 \to e^+e^-\nu) = 0.5$, which gives rise to events with up to two displaced dimuon vertices. To explore a wide range of kinematic variables and event topologies, we chose six $m(\tilde{q})$ values in the range between 125 GeV and 1.6 TeV, and for each chosen $m(\tilde{q})$, generated sets of samples with $\Delta m = m(\tilde{q}) - m(\tilde{\chi}_1^0)$ of 25, 200, and 650 GeV, and sets with constant $m(\tilde{\chi}_1^0)$ values of 50 and 500 GeV such that $m(\tilde{\chi}_1^0) < m(\tilde{q})$. To study a wide range of signal displacements, each set contains three samples with the generated $c\tau(\tilde{\chi}_1^0)$ values corresponding to mean transverse decay lengths of approximately 3, 30, and 250 cm in the laboratory frame. All other SUSY particles (e.g., gluinos and sleptons) are assumed to be too heavy to be produced. (Their masses are set to 10 TeV.) The samples are generated with PYTHIA 8.306. The squark-antisquark production cross sections are calculated with `NNLL-fast` version 2.0 to approximate next-to-next-to-leading order (NNLO) in the strong coupling constant, including the resummation of soft

gluon emission at next-to-next-to-leading logarithmic accuracy [25]. The computation uses the NNLO PDF4LHC21 parton distributions functions (PDFs) [26].

Since the optimization of the event selection criteria and the evaluation of the residual backgrounds are performed using data, the simulated background samples are used primarily to gain a better understanding of the nature and composition of background events passing the event selection. Simulated background samples used in the analysis include Drell–Yan (DY) dilepton production; $t\bar{t}$, tW, and $\bar{t}W$ events; W and Z boson pair production (dibosons); samples of J/ψ mesons produced in b hadron cascade decays; W+jets; and events comprised of jets produced through the strong interaction that are enriched in muons from semileptonic decays of hadrons containing b or c quarks.

The simulated signal and background samples are produced with PDFs NNPDF3.1 [27] at NNLO, using the CP5 tune [28], which is optimized for these PDFs, to model the underlying event. The passage of particles through the detector is simulated by GEANT4 [29]. Simulated minimum bias events are superimposed on a hard interaction in simulated events to describe the effect of additional inelastic pp interactions within the same or neighboring bunch crossings, known as pileup. All simulated events are then reconstructed with the same algorithms as used for data. A reweighting procedure that combines events in all simulated signal samples at a given signal mass [30] is employed to calculate the efficiencies for lifetimes different from those of the available samples.

4 Analysis strategy and event selection

4.1 Analysis strategy

An LLP produced in the hard interaction of the colliding protons may travel a significant distance in the detector before decaying into muons. While trajectories of the muons produced well within the silicon tracker can be reconstructed by both the tracker and the muon system, tracks of muons produced in the outer tracker layers or beyond can only be reconstructed by the muon system. Since the dimuon vertex resolution and the background composition differ dramatically depending on whether the muon is reconstructed in the tracker, we classify all reconstructed dimuon events into three mutually exclusive categories: a) both muons are reconstructed using both the tracker and the muon system (TMS-TMS category); b) both muons are reconstructed using only the muon system, as "standalone" muons (STA-STA category); and c) one muon is reconstructed only in the muon system, whereas the other muon is reconstructed using both the tracker and the muon system (STA-TMS category). These three categories of events are analyzed separately, with each benefiting from dedicated event selection criteria and background evaluation. The STA-TMS category, which had the lowest sensitivity among the three categories in the Run 2 analysis [5], is not used for the results presented in this paper; the results in the other two categories are statistically combined.

The beam spot is identified with the mean position of the pp interaction vertices. The primary vertex (PV) is taken to be the vertex corresponding to the hardest scattering in the event, evaluated using tracking information alone, as described in Section 9.4.1 of Ref. [31]. A pair of reconstructed muon tracks is fitted to a common secondary vertex (SV), which is expected to be displaced with respect to the PV. The transverse decay vector $\vec{L}_{xy}$ is defined from the PV to the SV in the plane transverse to the beam direction, while the transverse decay length L_{xy} is the magnitude of this vector. The transverse impact parameter d_0 is defined as the distance of closest approach of the muon track in the transverse plane with respect to the PV.

4.2 Trigger algorithms

Events were collected with dedicated triggers aimed at recording dimuons produced both within and outside of the tracker. In Run 2, these triggers required two muons reconstructed in the muon system alone, without using any information from the tracker [32]. They were deployed in 2016 and 2018 and included a beam spot constraint in the muon track fits at L1 but not at the HLT. The values of the L1 p_{T} thresholds varied from 11 and 4 GeV (for the leading and subleading L1 muons, respectively) during most of 2016 to 15 and 7 GeV at the end of Run 2. Each HLT muon was required to be within the region $|\eta| < 2.0$ and to have transverse momentum $p_{\mathrm{T}} > 28$ (23) GeV for 2016 (2018) data taking.

The primary goal of the trigger optimization performed for Run 3 data taking was to increase the signal efficiency by lowering as much as possible the p_{T} thresholds and by removing the beam spot constraint at L1, without increasing considerably the resulting trigger rate. Two additional sets of L1 triggers were introduced. One set comprises double-muon triggers with either no or a very low (4.5 GeV) muon-p_{T} threshold, which were made possible by requiring that the L1 muon candidates have opposite signs, segments in at least three different muon stations, angular separation $\Delta R_{\mu\mu} = \sqrt{(\Delta\eta_{\mu\mu})^2 + (\Delta\phi_{\mu\mu})^2}$ that does not exceed a threshold that varies between 1.2 and 1.4, and $|\eta| < 1.5$ in the trigger with no explicit p_{T} requirement. The other set takes advantage of a new track-finding procedure in the barrel section of the L1 muon trigger. This procedure enables the reconstruction of L1 muon candidates and the determination of their p_{T} without using the beam spot constraint [15]. These triggers require this p_{T} be larger than 15 and 7 GeV for the leading and subleading L1 muon, respectively. The p_{T} thresholds are lowered to 6 and 4 GeV when d_0 of both L1 muons is larger than 25 cm. The new L1 triggers mitigate the efficiency loss that was present in Run 2 for displaced muons not pointing to the beamspot [5], thereby improving the trigger efficiency for LLPs with $c\tau \gtrsim 10$ cm. The relative efficiency gain evaluated using the simulated HAHM signal events increases as $c\tau$ increases, reaching a plateau at 20 to 50% (depending on $m(\mathrm{Z_D})$) at $c\tau(\mathrm{Z_D}) \approx 10$ m.

The events selected by the aforementioned L1 triggers were then required to be selected by a logical OR of the 2018 L2 trigger paths used in the Run 2 analysis [5] and the newly designed HLT paths. The new paths use two complementary algorithms described below, and are characterized by p_{T} thresholds that depend on the muon d_0, as illustrated in Fig. 2. The first algorithm, labeled Run 3 (2022, L2) in Fig. 2, imports some of the elements of the offline analysis into the online selection, in order to take advantage of the superior tracker resolution in determining muon d_0. Instead of stopping the online reconstruction at the L2 stage (muon system alone) as it was done in the Run 2 trigger, the algorithm attempts to reconstruct the muon candidates at the L3 stage as well (similar to offline TMS muons). If either of the two L2 muon candidates is reconstructed at L3 as a muon with $d_0 < 1$ cm, the event is discarded, since such an L2 muon candidate is likely to originate from the background processes. The resulting trigger operates with muon p_{T} thresholds of 10 GeV and improves significantly the signal efficiency in the STA-STA category, while contributing only about 1% additional HLT rate.

The second new HLT algorithm, labeled Run 3 (2022, L3) in Fig. 2, introduces new paths relying entirely on the online L3 muon reconstruction. A moderate threshold on the impact parameter of each muon, $d_0 > 0.01$ cm, allows the p_{T} thresholds to be fairly low: 16 GeV on the leading muon μ_1 and 10 GeV on the subleading muon μ_2. The resulting trigger greatly improves the signal efficiency in the TMS-TMS category, while adding only another ≈1% of HLT rate. An increase in the number of background events selected by the trigger led to the refinements in the offline event selection described in Section 4.3.

The combined L1-HLT efficiency of the various displaced dimuon trigger paths and their com-

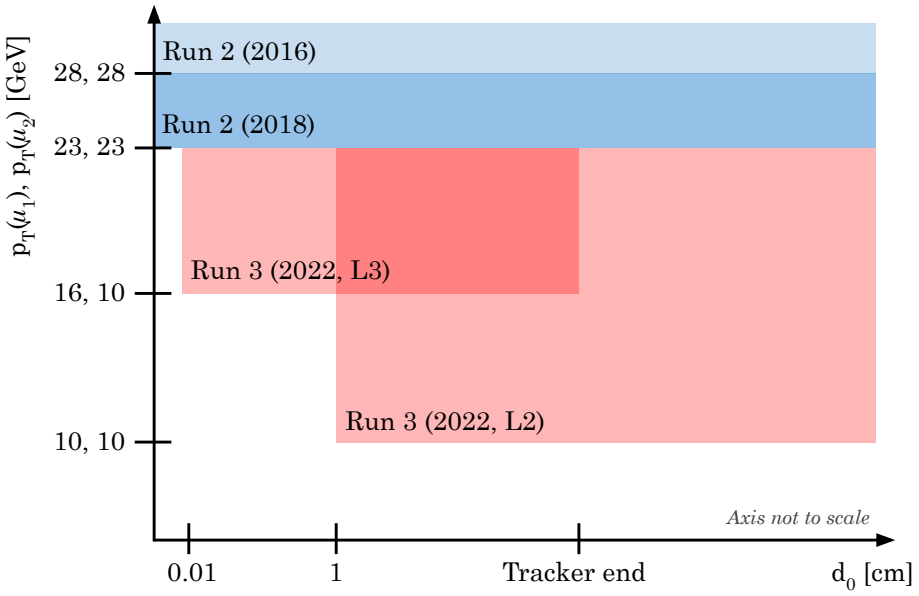

Figure 2: The p_T and d_0 coverage of the 2016 Run 2 triggers (light blue), 2018 Run 2 triggers (blue), and newly designed 2022 Run 3 triggers described in the text (red). The two values of the p_T refer to the trigger thresholds for the muons.

bination as a function of $c\tau$ is shown in Fig. 3 for the simulated HAHM signal events with $m(Z_D) = 20\,\text{GeV}$. Because the Run 2 triggers (dashed black) have no restrictions on d_0, they continue to have the highest efficiency (15%) at $c\tau < 0.02\,\text{cm}$. The addition of the Run 3 (2022, L3) paths (blue) increases the overall efficiency (black) by more than a factor of 2 for $c\tau = 0.1$–$1\,\text{cm}$. The efficiency of this trigger starts to drop at $c\tau \gtrsim 5\,\text{cm}$, when dimuons are produced beyond the innermost tracker layers and the L3 muon reconstruction efficiency decreases. At larger $c\tau$ values, the addition of the Run 3 (2022, L2) paths (red) strongly contributes to the improvement of the signal efficiency, e.g., by more than a factor of 3 at $c\tau = 1\,\text{m}$. The decline of the efficiencies at the largest $c\tau$ is driven by the increased fraction of dimuons produced outside the CMS detector. Overall, the addition of new L1 and HLT paths improves the trigger efficiency for Z_D with $m(Z_D) > 10\,\text{GeV}$ and $c\tau \gtrsim 0.1\,\text{cm}$ by a factor of 2 to 4, depending on $c\tau$ and mass. The performance of the trigger was validated using data as described in Section 6.

4.3 Muon reconstruction and event selection

Optimal performance for the wide range of displacements of secondary vertices considered in the analysis cannot be achieved by a single muon reconstruction algorithm. To accurately reconstruct muons produced near the IP, commonly used algorithms developed for prompt muons are employed. These algorithms combine measurements from both the tracker and the muon system. Two such TMS algorithms are the global muon and tracker muon reconstruction algorithms [13, 33]. The global muon algorithm reconstructs muons by fitting hits in the tracker and segments in the muon system into a common track. The tracker muon algorithm, on the other hand, builds muons by extrapolating tracks in the inner tracker to the muon system and requiring loose geometric matching to DT or CSC segments. However, the efficiency of these algorithms decreases rapidly as the distance between the IP and the muon origin increases. In contrast, algorithms that rely solely on information from the muon system can still efficiently

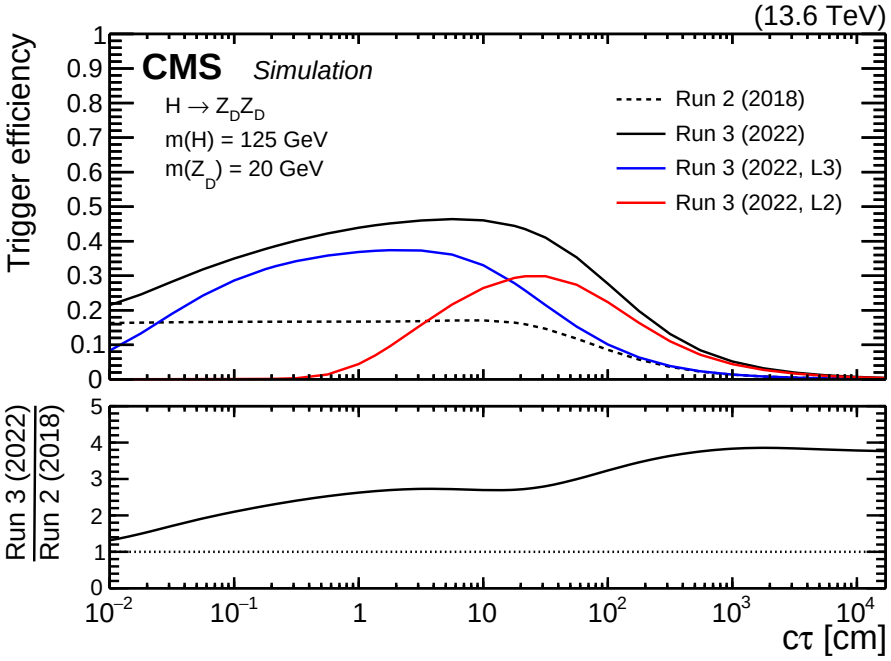

Figure 3: Efficiencies of the various displaced dimuon trigger paths and their combination as a function of $c\tau$ for the HAHM signal events with $m(\mathrm{Z_D}) = 20\,\mathrm{GeV}$. The efficiency is defined as the fraction of simulated events that satisfy the detector acceptance and the requirements of the following sets of trigger paths: the Run 2 (2018) triggers (dashed black); the Run 3 (2022, L3) triggers (blue); the Run 3 (2022, L2) triggers (red); and the OR of all these triggers (Run 3 (2022), black). The lower panel shows the ratio of the overall Run 3 (2022) efficiency to the Run 2 (2018) efficiency.

reconstruct muons produced in the outer tracker layers and beyond. These STA algorithms [13, 33] can reconstruct muons with displacements of up to a few meters. However, they exhibit poorer spatial and momentum resolution compared to muons reconstructed using the more precise information from the silicon tracker.

To benefit from the advantages offered by both types of algorithms, we begin the muon selection with the muons reconstructed by a specific STA algorithm that eliminates the beam spot constraints from all stages of the muon reconstruction procedure. This approach yields the highest efficiency and the finest resolution for highly displaced muons, surpassing all other available STA algorithms. Subsequently, we attempt to match each STA muon with muons reconstructed using global muon and tracker muon algorithms, and replace the STA muon with an associated TMS muon if a match is found. As in the Run 2 analysis [5], we reject events in which no HLT muon pair that triggered the event matches two STA muons.

Due to the need to reduce large backgrounds as much as possible, careful optimization of the event, muon, and dimuon selection was done for the Run 2 analysis, as described in Section 4 of Ref. [5]. A summary of the selection criteria used in the Run 2 analysis is given in Table 1 of Ref. [5]. Most of the selection criteria are unchanged, as is the association between STA and TMS muons for those tracks originating within the tracker volume. The rest of this section of the paper describes only the changes and refinements to the muon and dimuon selection for this Run 3 search, while also introducing analysis variables that are used in the background estimation.

Because of the increase in the background as a result of the lower p_{T} trigger thresholds, an iso-

lation requirement is useful when applied to the STA muons. Both STA muons in the STA-STA category are required to have relative tracker isolation $I^{\text{STA}}_{\text{rel, trk}} < 0.15$, where $I^{\text{STA}}_{\text{rel, trk}}$ is defined as the sum of the p_{T} of tracks within a cone of $\Delta R = \sqrt{(\Delta\eta)^2 + (\Delta\phi)^2} < 0.3$ around the trajectory of the muon extrapolated to the point of closest approach to the PV divided by the muon track p_{T}. When evaluated using events that pass all other selection criteria, this isolation requirement is more than 90% efficient for signal and suppresses background from events with jets that are produced through the strong interaction, collectively referred to as quantum chromodynamics (QCD) events, by about a factor of 2. The TMS muon isolation criterion, $I^{\text{TMS}}_{\text{rel, trk}} < 0.075$, remained unchanged with respect to the Run 2 analysis [5].

The Run 2 analysis required that the dimuons be displaced with respect to the PV by imposing requirements on the L_{xy} significance $L_{\text{xy}}/\sigma_{L_{\text{xy}}}$, where $\sigma_{L_{\text{xy}}}$ is the uncertainty in L_{xy} [5]. A significant fraction of remaining events in the STA-STA category suffer from unreliable SV reconstruction; we thus require in addition that $\sigma_{L_{\text{xy}}} < 20\,\text{cm}$.

In the TMS-TMS category, the sensitivity of the search is further improved by binning events in $\min(d_0/\sigma_{d_0})$, which is the minimum value of the ratio of d_0 to its uncertainty for the two muons forming a dimuon. Unlike signal events with macroscopic $c\tau$ values, the expected background has a steeply falling $\min(d_0/\sigma_{d_0})$ distribution, which motivates the splitting of the signal region (SR) into three bins of $\min(d_0/\sigma_{d_0})$ ranges. The bin ranges are the same as those in the Run 2 analysis, namely 6–10, 10–20, and >20.

A quantity that is useful for suppressing and evaluating the SM background that satisfies all other selection requirements is the azimuthal angle $\Delta\Phi$ between $\vec{L}_{\text{xy}}$ and the transverse momentum vector $\vec{p}_{\text{T},\mu\mu}$ of the dimuon system. A major source of SM background events is from prompt high-mass dimuons that are reconstructed as displaced due to instrumental or reconstruction failures. Such dimuons mostly arise from DY dimuon production. Events from DY $\tau^+\tau^-$ production with both τ leptons decaying to muons lead to a background with characteristics similar to those of the mismeasured DY $\mu^+\mu^-$ events; contributions from processes such as $\text{t}\bar{\text{t}}$ and diboson production are relatively small. Dimuons originating in these events, collectively referred to as DY events, are expected to have a distribution of $|\Delta\Phi|$ symmetric about $\pi/2$, because the dimuon momentum vector is uncorrelated with the $\vec{L}_{\text{xy}}$ vector. On the other hand, when a pair of muons is produced in the decay of an LLP originating at the PV, the resulting $\vec{p}_{\text{T},\mu\mu}$ and $\vec{L}_{\text{xy}}$ are collinear, and the distribution of $|\Delta\Phi|$ peaks at zero. This can be seen in Fig. 4, which compares the $|\Delta\Phi|$ distributions of TMS-TMS and STA-STA dimuons in data samples obtained by inverting some of the selection criteria and enriched in DY events with the $|\Delta\Phi|$ distributions for events passing the full selection except for the $|\Delta\Phi|$ requirement in all HAHM and RPV SUSY signal samples combined. There is a small asymmetry in the $|\Delta\Phi|$ distribution for DY events in the STA-STA category, which is caused by the event selection criteria.

To address the different $|\Delta\Phi|$ distributions in the two types of signal models, we define different critical values $|\Delta\Phi|_{\text{C}}$ for requiring $|\Delta\Phi| < |\Delta\Phi|_{\text{C}}$. To define the SR for the HAHM model, where $|\Delta\Phi|$ strongly peaks at zero and the tail is driven by the resolution, we use $|\Delta\Phi|_{\text{C}} = \pi/10$ in the STA-STA category and $\pi/30$ in the TMS-TMS category. The tighter requirement in the TMS-TMS category takes advantage of the better tracker resolution. For the RPV SUSY model, where the distribution is broader due to the undetected neutrino among the decay products, we use a looser requirement of the Run 2 analysis, $|\Delta\Phi|_{\text{C}} = \pi/4$, in both dimuon categories. For the chosen $|\Delta\Phi|_{\text{C}}$ values, the signal efficiency is 90–99% in the HAHM and 60–99% in the RPV SUSY models, depending on the Lorentz boost of the LLP; the corresponding DY background rejection factors are, respectively, 15–20 and 4–6, depending on the dimuon category. We use the

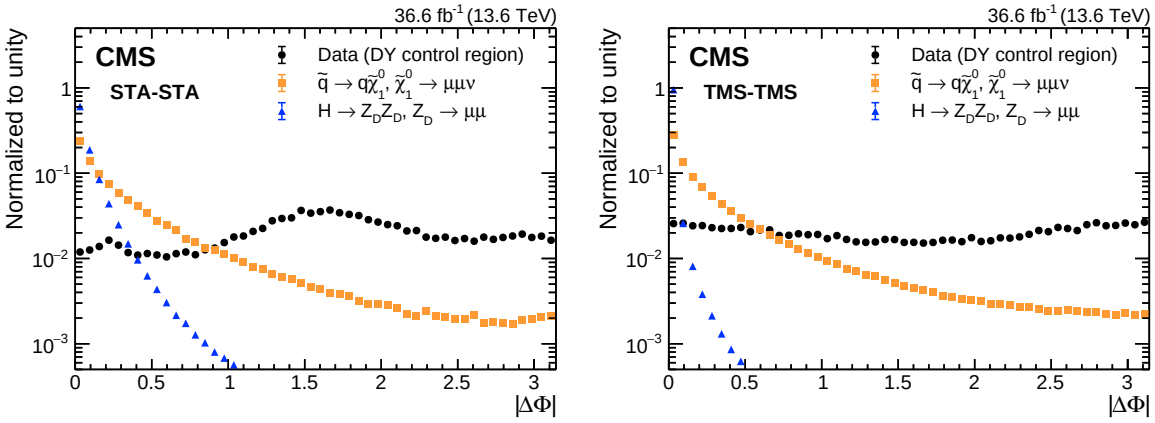

Figure 4: Distributions of $|\Delta\Phi|$ for (left) STA-STA and (right) TMS-TMS dimuons in data samples obtained by inverting some of the selection criteria and enriched in DY events (black circles) and for events passing all selection criteria except for a requirement on $|\Delta\Phi|$ in all HAHM (blue triangles) and RPV SUSY (orange squares) generated signal samples combined. All distributions are normalized to unit area.

symmetric region, $|\Delta\Phi| > \pi - |\Delta\Phi|_C$, as a control region (CR) for evaluating the contribution from DY and other prompt backgrounds, and the validation regions (VR) with $\pi/4 < |\Delta\Phi| < \pi/2$ and $\pi/2 < |\Delta\Phi| < 3\pi/4$ for validating background predictions, as discussed in Section 5.

In addition to defining $|\Delta\Phi|$ SR and CRs, we classify selected dimuons as opposite-sign (OS) or same-sign (SS), based on the observed muon charges. The signal selection requires that dimuons be OS, while SS dimuons constitute a CR used to evaluate backgrounds arising from QCD events.

The last important source of SM backgrounds consists of QCD events in which there are dimuons produced in decays of J/ψ mesons and other low-mass SM resonances, or formed from the products of the b hadron cascade decays ($b \to c\mu_1 X$ followed by $c \to \mu_2 X$). These events are suppressed by requiring that $m_{\mu\mu} > 10\,\text{GeV}$. However, it was observed that low-p_T muons can appear as muons with higher p_T, with straighter tracks, when reconstructed from a small number of measurements. This gives rise to dimuons with an overestimated $m_{\mu\mu}$ (above the 10 GeV threshold) and a mistakenly formed displaced vertex. These dimuons typically have small $|\Delta\Phi|$ (either due to the collinearity of the $\vec{p}_{T,\mu\mu}$ and $\vec{L}_{xy}$ vectors or overestimated muon p_T) and may exhibit large values of $L_{xy}/\sigma_{L_{xy}}$ and d_0/σ_{d_0} that resemble signal-like characteristics. To suppress such events, which are particularly abundant in the STA-STA category due to its low resolution, we reject STA-STA dimuons whose separation in η is small ($|\Delta\eta_{\mu\mu}| < 0.1$) if one of the muons is reconstructed in the barrel from fewer than 25 DT hits or if the sum of the segments belonging to both muons in the dimuon is fewer than 6. These requirements are identical to those used in the Run 2 analysis.

Finally, to test for the existence of an LLP with a given mass, dimuons satisfying the selection criteria are required to have $m_{\mu\mu}$ within a specified interval containing the probed LLP mass. The width of each interval is chosen according to the mass resolution and the expected background. For the interpretation in the framework of the HAHM model, where the LLP decay products do not contain any undetected particles, the full widths of the chosen $m_{\mu\mu}$ intervals are approximately equal to 6–8 times the mass resolution at this mass. This choice typically yields intervals containing a large fraction (90–99%) of putative signal with the probed mass. Since the mass resolution in the TMS-TMS category is far superior to that in the STA-STA category (1–3% compared to 10–25%, for LLP masses between 20 and 350 GeV), the minimum

width of $m_{\mu\mu}$ intervals varies from 3 GeV in the TMS-TMS category to ≈20 GeV in the STA-STA category.

In the RPV SUSY model, the presence of a neutrino in the $\widetilde{\chi}_1^0 \to \mu^+\mu^-\nu$ decay vertex leads to a nonpeaking dimuon invariant mass distribution with an endpoint at $m(\widetilde{\chi}_1^0)$. To improve the mass resolution and the signal-to-background discrimination in signals featuring an LLP decay vertex formed by a dimuon plus neutral or unobserved particles, we use the quantity referred to as the corrected SV mass, defined as

$$m_{\mu\mu}^{\text{corr}} = \sqrt{m_{\mu\mu}^2 + p_{\mu\mu}^2 \sin^2\theta} + p_{\mu\mu}\sin\theta, \tag{1}$$

where $p_{\mu\mu}$ is the magnitude of the dimuon momentum vector $\vec{p}_{\mu\mu}$, and θ is the angle between $\vec{p}_{\mu\mu}$ and the vector connecting the PV with the SV. The motivation behind this variable, which was used at LEP and the SLC and recently by LHCb [34] and CMS [35], is to rely on the conservation of momentum and correct for the missing mass of the vertex due to unaccounted particles. In the case where only the dimuon belongs to the LLP decay vertex (and before measurement error), $\theta = 0$ and $m_{\mu\mu}^{\text{corr}} = m_{\mu\mu}$. If, however, the decay vertex includes other particles, then $\theta > 0$, $m_{\mu\mu}^{\text{corr}} > m_{\mu\mu}$, and the corrected mass is the minimum mass that the LLP, in this case the $\widetilde{\chi}_1^0$, can have in order to be consistent with the measured direction of flight. The $m_{\mu\mu}^{\text{corr}}$ distributions of simulated RPV SUSY events show a clear peak at $m(\widetilde{\chi}_1^0)$ in both dimuon categories. We profit from the improvement in mass resolution offered by $m_{\mu\mu}^{\text{corr}}$ and use $m_{\mu\mu}^{\text{corr}}$ intervals to probe different $m(\widetilde{\chi}_1^0)$. As with $m_{\mu\mu}$ intervals for the HAHM model, the width of the intervals is chosen to contain a large fraction of the RPV SUSY signal (typically 80–90%). In the STA-STA category, we additionally require $m_{\mu\mu} > 15$ GeV to avoid the leakage of background events from small $m_{\mu\mu}$ to large $m_{\mu\mu}^{\text{corr}}$.

Figure 5 shows, as an example, the full event selection efficiency for the HAHM signal with $m(\text{Z}_\text{D}) = 20$ GeV as a function of $c\tau$, and illustrates relative improvements in the efficiencies from the new trigger algorithms. A large increase in the overall efficiency, shown in the lower panel, is apparent; most of the efficiency gain from the improvements in the trigger algorithms and shown in Fig. 3 is retained after the full offline event selection. Similar efficiency increases are seen at other probed Z_D masses.

5 Background estimates and their systematic uncertainties

Background events that meet the event selection criteria cannot be reliably simulated since they consist of misreconstructed prompt muons and muons in jets. Therefore, we rely on analyzing events in the recorded data to estimate the expected background. To achieve this, we employ CRs where one or more selection criteria are inverted, creating a region predominantly populated by a specific type of background while having an insignificant contribution from the signal processes. The specific definitions of these CRs and the procedure for evaluating the background differ across dimuon categories and are elaborated on in the rest of this section. The background evaluation methods are nearly all identical to those employed in the Run 2 analysis [5]. The only exception is the evaluation of QCD backgrounds in the STA-STA category, which can now benefit from events rejected by the new STA muon isolation requirement. In order to prevent potential bias in the event selection, the events that satisfy the full set of selection criteria (i.e., those in the SR) were kept concealed (”blinded”) until the final stages of the analysis.

One particular type of background events arises from cosmic ray muons crossing the detector within the acceptance of the muon system. Such muons are often reconstructed as two back-to-

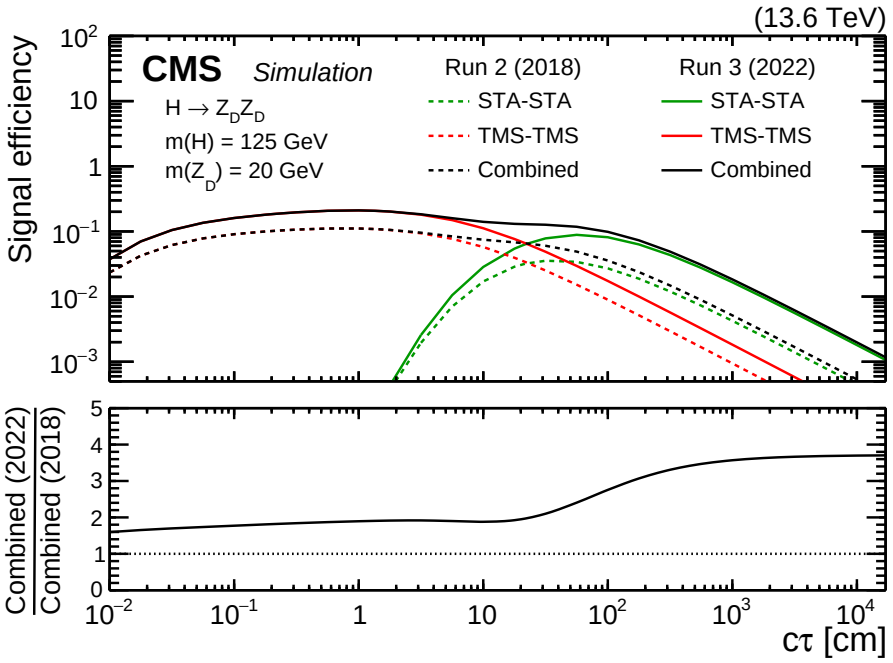

Figure 5: Overall efficiencies in the STA-STA (green) and TMS-TMS (red) dimuon categories, as well as their combination (black) as a function of $c\tau$ for the HAHM signal events with $m(\mathrm{Z_D}) = 20\,\mathrm{GeV}$. The solid curves show efficiencies achieved with the 2022 Run 3 triggers, whereas dashed curves show efficiencies for the subset of events selected by the triggers used in the 2018 Run 2 analysis. The efficiency is defined as the fraction of signal events that satisfy the criteria of the indicated trigger as well as the full set of offline selection criteria. The lower panel shows the relative improvement of the overall signal efficiency brought in by improvements in the trigger.

back muons, one in the upper half and one in the lower half of the detector. For each dimuon category, the contribution from cosmic ray muons is assessed independently by examining the number of dimuons that meet all the selection criteria except for angular requirements designed to reject putative dimuons that are formed from back-to-back muons [5]. To evaluate this contribution, we use the rejection factors of these requirements, which are determined from a sample of cosmic ray muons recorded during periods without any beam activity. In both dimuon categories, the remaining background originating from cosmic ray muons is estimated to be less than 0.1 events in all mass intervals combined.

5.1 Estimation of Drell–Yan and other prompt backgrounds

The contribution from misreconstructed prompt high-mass dimuons, mainly originating from the DY process, to the total background is evaluated from events in the signal-free $|\Delta\Phi|$-symmetric CR as

$$N^{i}_{\mathrm{DY}}(\mathrm{OS};|\Delta\Phi| < |\Delta\Phi|_{\mathrm{C}}) = N^{i}_{\mathrm{DY}}(\mathrm{OS};|\Delta\Phi| > \pi - |\Delta\Phi|_{\mathrm{C}})R^{i}_{\mathrm{DY}}, \tag{2}$$

where $N^{\mathrm{i}}_{\mathrm{DY}}(\mathrm{OS};|\Delta\Phi| < |\Delta\Phi|_{\mathrm{C}})$ and $N^{\mathrm{i}}_{\mathrm{DY}}(\mathrm{OS};|\Delta\Phi| > \pi - |\Delta\Phi|_{\mathrm{C}})$ are, respectively, the numbers of DY background events in the SR and its $|\Delta\Phi|$-symmetric CR with $|\Delta\Phi|_{\mathrm{C}}$ representing the selection criterion applied; R^{i}_{DY} is the transfer factor accounting for the residual asymmetry in the population of events in the two $|\Delta\Phi|$ regions and obtained from auxiliary measurements; and the index i denotes the dimuon category (STA-STA or TMS-TMS). The number of DY dimuons in the CR is obtained from the total number of events in that region corrected by the expected contribution from QCD background events, estimated as discussed in Section 5.2.

To assess the symmetry of the $|\Delta\Phi|$ distributions in this class of background events, events in dedicated CRs are used. In the STA-STA category, we focus on events within data CRs that are obtained by reversing the STA-to-TMS association. Specifically, we select events where STA-STA dimuons satisfy all the selection criteria, except that each of the constituent STA muons is associated with a TMS muon. To ensure that these STA-STA dimuons are promptly produced (and not part of the signal), we require that the associated TMS-TMS dimuons, which offer superior spatial resolution, are prompt. This is achieved by imposing $L_{xy}/\sigma_{L_{xy}} < 1.0$ for the associated TMS-TMS dimuon. To minimize contamination from muons originating from jets (which are discussed separately below), each TMS muon in the associated TMS-TMS dimuon is required to have $I^{\text{TMS}}_{\text{rel, trk}} < 0.05$. From this sample, we obtain $R^{\text{STA-STA}}_{\text{DY}} = 0.75 \pm 0.02$ (stat.) for $|\Delta\Phi|_{\text{C}} = \pi/10$ and $R^{\text{STA-STA}}_{\text{DY}} = 0.73 \pm 0.02$ (stat.) for $|\Delta\Phi|_{\text{C}} = \pi/4$. The value of $R^{\text{TMS-TMS}}_{\text{DY}}$ is set to unity based on studies using simulation and data [5].

In both STA-STA and TMS-TMS categories, no significant dependence of the transfer factor R^{i}_{DY} on reconstructed dimuon mass is observed, and a single value is used for all signal mass intervals. The systematic uncertainties in $R^{\text{STA-STA}}_{\text{DY}}$ are assessed by comparing $R^{\text{STA-STA}}_{\text{DY}}$ measured in individual mass intervals with the result of the inclusive measurement and by varying the boundaries and definitions of the auxiliary CRs. The latter includes repeating the measurements of $R^{\text{STA-STA}}_{\text{DY}}$ in the region with only one STA-to-TMS association. Based on these studies, we assign a systematic uncertainty of 30% in $R^{\text{STA-STA}}_{\text{DY}}$. The systematic uncertainty in $R^{\text{TMS-TMS}}_{\text{DY}}$ is assigned to be 15% based on the studies of the residual $|\Delta\Phi|$ asymmetry for events in the $\min(d_0/\sigma_{d_0})$ and $|\Delta\Phi|$ side bins.

5.2 Estimation of QCD backgrounds

Many of the background processes yielding small-$|\Delta\Phi|$ OS dimuons also give rise to small-$|\Delta\Phi|$ SS dimuons, either because these processes are charge symmetric or via muon charge misassignment. Most of these dimuons are embedded in jets and are suppressed by the muon isolation requirements. Thus, we evaluate the contribution from the QCD backgrounds to the SR from events in CRs obtained by inverting two independent selection requirements: the isolation requirement (i.e., we select events where at least one of the muons fails to satisfy the isolation criteria used in the analysis) and the requirement of the OS dimuons (i.e., we select SS dimuons).

In the STA-STA category, we base our estimate of the QCD backgrounds on the number of events with OS nonisolated dimuons, using

$$N^{\text{STA-STA}}_{\text{QCD}}(\text{OS}; |\Delta\Phi| < |\Delta\Phi|_{\text{C}}) = N^{\text{STA-STA}}_{\text{noniso}}(\text{OS}; |\Delta\Phi| < |\Delta\Phi|_{\text{C}}) R^{\text{STA-STA}}_{\text{QCD}}, \tag{3}$$

where $N^{\text{STA-STA}}_{\text{QCD}}(\text{OS}; |\Delta\Phi| < |\Delta\Phi|_{\text{C}})$ and $N^{\text{STA-STA}}_{\text{noniso}}(\text{OS}; |\Delta\Phi| < |\Delta\Phi|_{\text{C}})$ are, respectively, the numbers of OS isolated and nonisolated dimuons with small $|\Delta\Phi|$, and $R^{\text{STA-STA}}_{\text{QCD}}$ is the transfer factor between these numbers. The transfer factor is evaluated using SS dimuons in the same small-$|\Delta\Phi|$ region:

$$R^{\text{STA-STA}}_{\text{QCD}} = \frac{N^{\text{STA-STA}}_{\text{iso}}(\text{SS}; |\Delta\Phi| < |\Delta\Phi|_{\text{C}})}{N^{\text{STA-STA}}_{\text{noniso}}(\text{SS}; |\Delta\Phi| < |\Delta\Phi|_{\text{C}})}, \tag{4}$$

with $N^{\text{STA-STA}}_{\text{iso}}(\text{SS}; |\Delta\Phi| < |\Delta\Phi|_{\text{C}})$ and $N^{\text{STA-STA}}_{\text{noniso}}(\text{SS}; |\Delta\Phi| < |\Delta\Phi|_{\text{C}})$ representing the numbers of, respectively, isolated and nonisolated SS STA-STA dimuons with $|\Delta\Phi| < |\Delta\Phi|_{\text{C}}$. To improve the precision of the $R^{\text{STA-STA}}_{\text{QCD}}$ measurement, we enlarge the sample of SS dimuons by removing tight requirements on the numbers of DT hits and muon segments applied to dimuons with $|\Delta\eta_{\mu\mu}| < 0.1$ (discussed in Section 4) as well as the generic requirement on the minimum number of DT hits [5]. We obtain $R^{\text{STA-STA}}_{\text{QCD}}$ values varying between 1.0 and 1.5 as a function of

reconstructed dimuon mass and measured with an uncertainty of 20–40%. They are in good agreement with $R_{\text{QCD}}^{\text{STA-STA}}$ values obtained from a sample of OS small-$|\Delta\Phi|$ events failing the criteria for dimuons with $|\Delta\eta_{\mu\mu}| < 0.1$. Systematic uncertainties arising from these two measurements are found to be much smaller than statistical uncertainties resulting from CR sample sizes.

Based on the Run 2 studies [5], we do not anticipate a significant contribution from $|\Delta\Phi|$-asymmetric low-mass dimuons in the TMS-TMS category. This is primarily due to the superior dimuon invariant mass resolution in this category. However, since there may still be a small contribution from $|\Delta\Phi|$-asymmetric dimuons, we prefer not to rely solely on the symmetry of $|\Delta\Phi|$ in evaluating the background. Consequently, the method used is similar to that employed in the STA-STA category and bases our estimate of the QCD backgrounds on the number of SS dimuons, using

$$N_{\text{QCD}}^{\text{TMS-TMS}}(\text{OS}; |\Delta\Phi| < |\Delta\Phi|_{\text{C}}) = N^{\text{TMS-TMS}}(\text{SS}; |\Delta\Phi| < |\Delta\Phi|_{\text{C}}) R_{\text{QCD}}^{\text{TMS-TMS}}. \quad (5)$$

The transfer factor $R_{\text{QCD}}^{\text{TMS-TMS}}$ is obtained from the ratio of OS to SS dimuons in the CR with the muon isolation requirement reversed, which consists of dimuons passing the nominal event selection but with at least one muon with $I_{\text{rel, trk}}^{\text{TMS}} > 0.075$ and both with $I_{\text{rel, trk}}^{\text{TMS}} < 0.5$. We have verified that these events, as well as SS dimuons passing isolation requirements, contain negligible contributions from signal and DY events. As the SR is divided into several $\min(d_0/\sigma_{d_0})$ bins, the evaluation of $R_{\text{QCD}}^{\text{TMS-TMS}}$ is performed separately in each $\min(d_0/\sigma_{d_0})$ bin. Since no significant dependence of the value of $R_{\text{QCD}}^{\text{TMS-TMS}}$ on $m_{\mu\mu}$ and $m_{\mu\mu}^{\text{corr}}$ is observed, $R_{\text{QCD}}^{\text{TMS-TMS}}$ in each $\min(d_0/\sigma_{d_0})$ bin is calculated by integrating events in the entire invariant mass spectrum. The measured values of $R_{\text{QCD}}^{\text{TMS-TMS}}$ decrease from 2.0 to 1.3 as $\min(d_0/\sigma_{d_0})$ increases, with the statistical uncertainties in the range 5–15%. A systematic uncertainty of 15% is assigned to account for variations of $R_{\text{QCD}}^{\text{TMS-TMS}}$ as a function of the invariant mass and as the result of varying the definition and boundaries of the auxiliary CR.

To avoid potential overestimation of the DY backgrounds, we use the same QCD background evaluation technique for dimuons in the CR defined by $|\Delta\Phi| > \pi - |\Delta\Phi|_{\text{C}}$. The obtained estimate of the QCD backgrounds is subtracted from the total to derive the estimate of DY dimuons in this $|\Delta\Phi|$ region, which is used for the evaluation of the DY backgrounds in the SR according to Eq. (2). This procedure is not applied in the STA-STA category, where the $|\Delta\Phi|$-symmetric QCD background is negligible. The sum of the QCD and DY background estimates constitutes the total predicted background in the SR. According to the background evaluation method, the DY backgrounds are expected to dominate at small d_0/σ_{d_0} and $L_{\text{xy}}/\sigma_{L_{\text{xy}}}$ values, whereas the relative QCD contribution becomes larger as d_0/σ_{d_0} and $L_{\text{xy}}/\sigma_{L_{\text{xy}}}$ increase. The uncertainty in the background predictions is mainly driven by the statistical uncertainty arising from the limited number of events observed in the CRs.

5.3 Validation of background predictions

To ensure the reliability of the background evaluation method described in Sections 5.1 and 5.2, we examine the method's performance in various VRs, which are chosen to have minimal or no contribution from the signal being studied. Thus, we can verify that it accurately predicts the background and that any observed discrepancies are within acceptable limits.

The evaluation of DY backgrounds is examined in the VRs obtained by inverting the $L_{\text{xy}}/\sigma_{L_{\text{xy}}}$ and d_0/σ_{d_0} requirements and thereby enriched in this class of events. An example is shown in Fig. 6, which compares the background predictions to the observed distributions in the

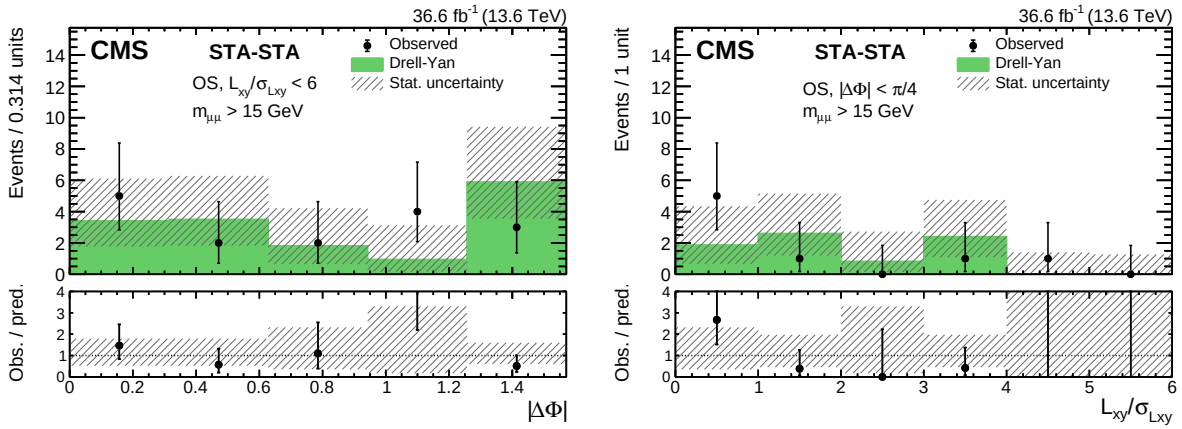

Figure 6: Example of background prediction checks in the STA-STA category: distributions of (left) $|\Delta\Phi|$ and (right) $L_{xy}/\sigma_{L_{xy}}$ for events with $m_{\mu\mu} > 15\,\text{GeV}$ in the $L_{xy}/\sigma_{L_{xy}} < 6$ validation region in data (black circles) compared to the background predictions (histograms). The lower panels show the ratio of the observed to predicted number of events. Hatched histograms show the statistical uncertainty in the background prediction.

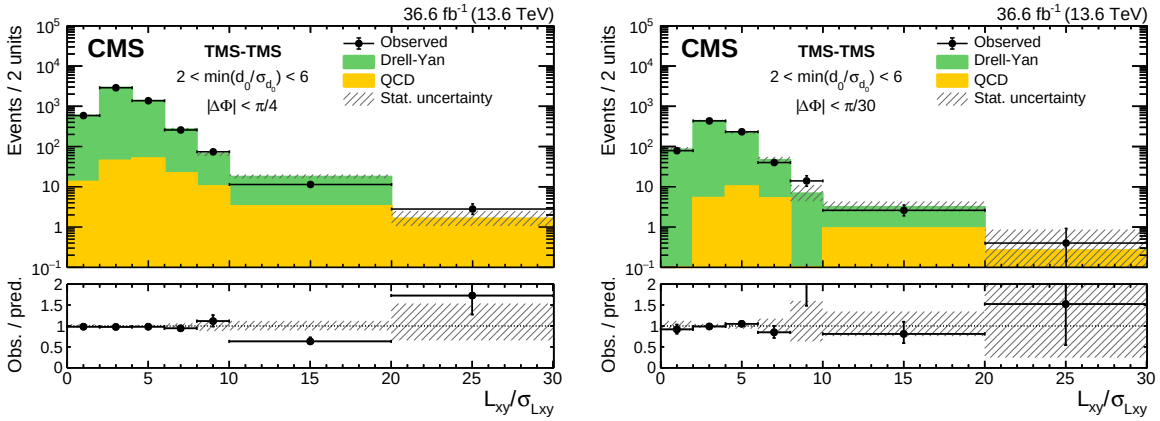

Figure 7: Example of background prediction checks in the TMS-TMS category: $L_{xy}/\sigma_{L_{xy}}$ distributions for events with (left) $|\Delta\Phi| < \pi/4$ and (right) $|\Delta\Phi| < \pi/30$ in the $2 < \min(d_0/\sigma_{d_0}) < 6$ validation regions compared to the background predictions. The number of observed events (black circles) is overlaid with stacked histograms showing the expected numbers of QCD (yellow) and DY (green) background events. The last bin includes events in the histogram overflow. The lower panels show the ratio of the observed to predicted number of events. Hatched histograms show the statistical uncertainty in the background prediction.

$L_{xy}/\sigma_{L_{xy}} < 6$ VR for dimuons with $m_{\mu\mu} > 15\,\text{GeV}$ in the STA-STA category. To check how the validity of the method depends on $|\Delta\Phi|$ and the dimuon displacement, we perform the evaluation of the background in corresponding bins. The expected number of background events in the given VR is computed according to Eq. (2) separately in each $|\Delta\Phi|$ or $L_{xy}/\sigma_{L_{xy}}$ bin and compared to the observed data. The predictions of the method are consistent with the yields in data.

In the TMS-TMS category, we apply the background evaluation procedure to the TMS-TMS dimuons in the VR defined by $2 < \min(d_0/\sigma_{d_0}) < 6$. The comparison of the predicted background and data in bins of $L_{xy}/\sigma_{L_{xy}}$ for two $|\Delta\Phi|_C$ requirements is shown in Fig. 7. The expected and observed numbers of events are in agreement in the entire probed $L_{xy}/\sigma_{L_{xy}}$ range.

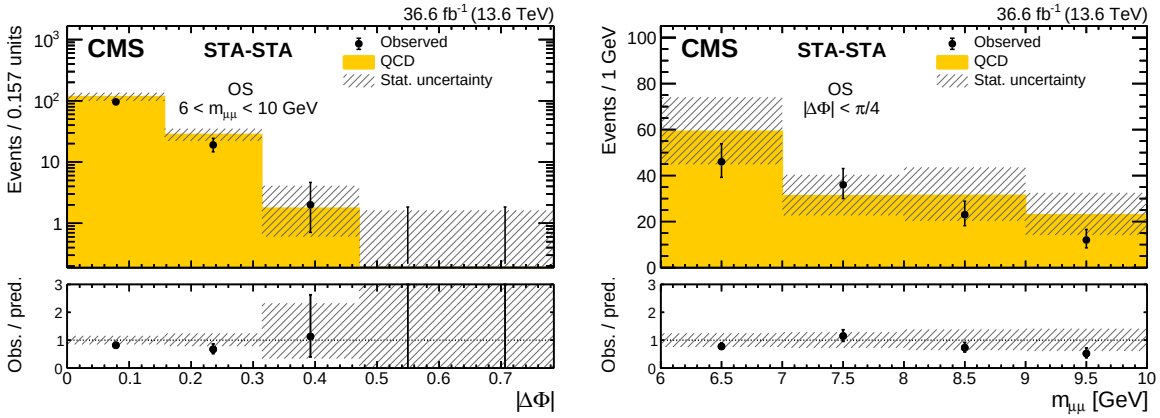

Figure 8: Example of background prediction checks in the STA-STA category: distributions of (left) $|\Delta\Phi|$ and (right) $m_{\mu\mu}$ for dimuons in the low-mass ($6 < m_{\mu\mu} < 10\,\text{GeV}$) validation region in data (black circles) compared to the background predictions (histograms). The lower panels show the ratio of the observed to predicted number of events. Hatched histograms show the statistical uncertainty in the background prediction.

The evaluation of the $|\Delta\Phi|$-asymmetric component of the background, which is particularly important in the STA-STA category, is tested in the low-mass ($6 < m_{\mu\mu} < 10\,\text{GeV}$) VR where the QCD backgrounds dominate. Figure 8 shows a comparison of predicted and measured background in this VR as a function of $|\Delta\Phi|$ and $m_{\mu\mu}$ for STA-STA dimuons. The yields in data are found to be consistent with the background predictions in all $|\Delta\Phi|$ and $m_{\mu\mu}$ intervals.

Finally, to ensure the validity of the method at different values of the main discriminating variables in the TMS-TMS category, the validation checks are performed in bins of $\min(d_0/\sigma_{d_0})$ and $m_{\mu\mu}$ of TMS-TMS dimuons. Such checks include comparisons in the d_0/σ_{d_0} sideband ($2 < d_0/\sigma_{d_0} < 6$) in the $|\Delta\Phi| < \pi/4$ SR, as well as those in the entire d_0/σ_{d_0} range in the $|\Delta\Phi|$ sideband, $\pi/4 < |\Delta\Phi| < \pi/2$. In the latter, the region with $\pi/4 < |\Delta\Phi| < \pi/2$ is used as a signal-free proxy for the $|\Delta\Phi| < \pi/4$ SR. The background evaluation procedure is applied to the OS and SS dimuons in the $|\Delta\Phi|$-symmetric region, $\pi/2 < |\Delta\Phi| < 3\pi/4$, as well as SS dimuons with $\pi/4 < |\Delta\Phi| < \pi/2$. The comparisons of the predicted background and data as a function of $\min(d_0/\sigma_{d_0})$ and $m_{\mu\mu}$ for TMS-TMS dimuons in these VRs are shown in Fig. 9. The observed and expected numbers of events are consistent within statistical uncertainties.

6 Systematic uncertainties affecting signal

The modeling of signal efficiencies in simulation was extensively studied in the Run 2 search [5]. Since no changes affecting this analysis were made in the CMS detector or in the muon reconstruction algorithms between Run 2 and Run 3, many of the systematic uncertainties and data-to-simulation corrections are taken directly from Ref. [5]. New studies include modeling of signal efficiencies related to the new trigger algorithms and modified event selection criteria, such as the STA muon isolation. The studies are performed for each dimuon category separately, using dedicated data samples. Unless stated otherwise, we consider sources of uncertainties to be uncorrelated between different categories.

In both categories, the dominant systematic uncertainties and the largest data-to-simulation corrections arise from muon identification, muon reconstruction, and trigger efficiencies. At small displacements, the systematic effects related to these efficiencies are examined as a function of muon p_{T} and η by applying the "tag-and-probe" method [33] to prompt muons from J/ψ

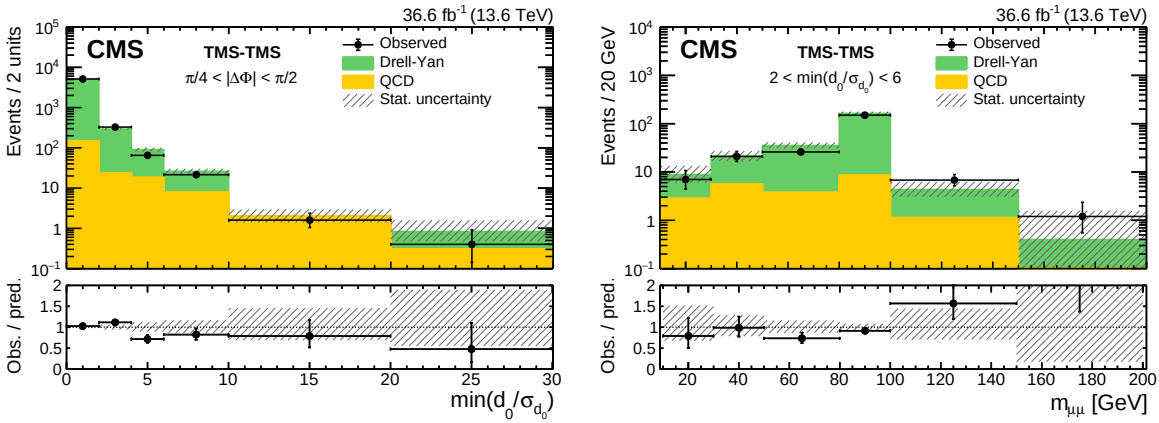

Figure 9: Example of background prediction checks in the TMS-TMS category: (left) distribution of $\min(d_0/\sigma_{d_0})$ for events in the $\pi/4 < |\Delta\Phi| < \pi/2$ validation region; (right) distribution of $m_{\mu\mu}$ for events in the $2 < \min(d_0/\sigma_{d_0}) < 6$ validation region. The number of observed events (black circles) is overlaid with stacked histograms showing the expected numbers of QCD (yellow) and DY (green) background events. The last bin includes events in the histogram overflow. The lower panels show the ratios of the observed to predicted number of events. Hatched histograms show the statistical uncertainty in the background prediction.

meson and Z boson decays. The evolution of efficiencies as a function of displacement is studied using cosmic ray muons and muons from decays of nonprompt J/ψ mesons. These studies yield corrections to the simulated signal yields that range, depending on the signal sample, from 0.75 to unity for the STA-STA category and from 0.83 to unity for the TMS-TMS category. The overall uncertainty increases continuously with displacement, from ≈5% for prompt-like muons to ≈15% for muons with $d_0 = 100\,\text{cm}$, reflecting the precision of studies using cosmic ray muons. Since a large part of this uncertainty stems from the evaluation of efficiencies of trigger algorithms common to both dimuon categories, it is taken as correlated between the categories.

Dedicated studies were performed to examine the effect of the d_0 thresholds and looser muon p_T requirements of the new displaced dimuon triggers. The efficiency of the Run 3 (2022, L3) triggers is evaluated using dimuons from decays of nonprompt J/ψ mesons selected by the triggers that use jets and event p_T imbalance. As a result of these studies, the simulated yields of signal events selected by this set of triggers are scaled by a factor of 0.95, and an uncertainty of 5% is assigned. The efficiency of the Run 3 (2022, L2) triggers is studied using cosmic ray muons. While no systematic biases are observed, the largest data-simulation difference of 3% in bins of d_0 is assigned as a systematic uncertainty in the efficiency of these triggers. These corrections and uncertainties are included in the overall corrections and uncertainties discussed in the previous paragraph.

The accuracy of the modeling of the muon isolation requirements is assessed using muons from Z boson decays and, in the case of STA muons, cosmic ray muons selected in pp collision events. Based on the results of these studies, a systematic uncertainty of 6 (2)% is assigned to the efficiency of STA (TMS) muons. The uncertainty in the Higgs boson production cross section at 13.6 TeV amounts to $^{+5\%}_{-7\%}$ [21]. The remaining systematic uncertainties, e.g., those related to muon p_T resolution and dimuon vertex reconstruction, are less than 5%. The uncertainty in the integrated luminosity is 2.3% [36]. The uncertainty in the signal efficiency due to pileup modeling is 2%. Both luminosity and pileup uncertainties are correlated among the dimuon categories.

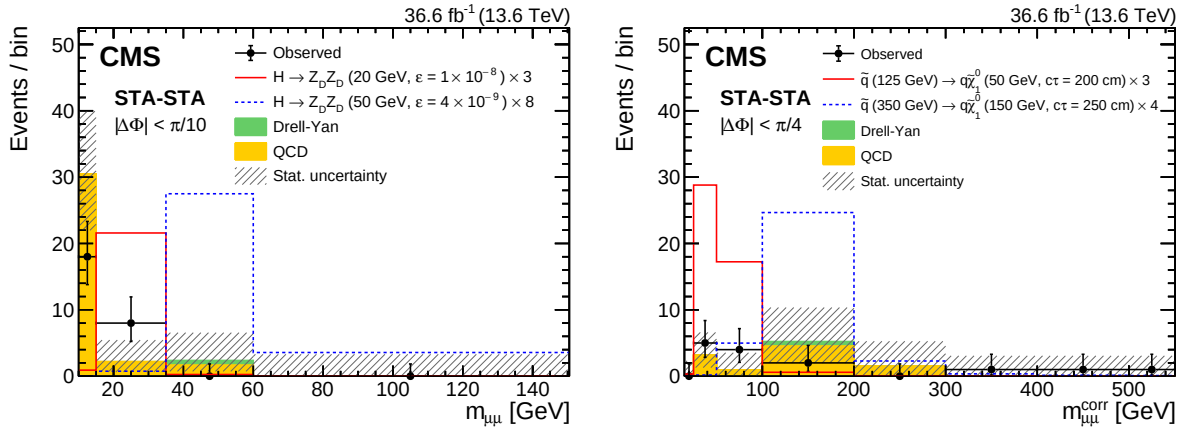

Figure 10: Comparison of the observed (black points) and expected (histograms) numbers of events in nonoverlapping (left) $m_{\mu\mu}$ and (right) $m_{\mu\mu}^{\text{corr}}$ intervals in the STA-STA dimuon category, in the signal regions optimized for the (left) HAHM and (right) RPV SUSY model. Yellow and green stacked filled histograms represent mean expected background contributions from QCD and DY, respectively, while statistical uncertainties in the total expected background are shown as hatched histograms. Signal contributions expected from simulated signals indicated in the legends are shown in red and blue. Their yields are set to the corresponding median expected 95% CL exclusion limits obtained from the ensemble of both dimuon categories, scaled up as indicated in the legend to improve visibility. The last bin includes events in the histogram overflow.

7 Results

The numbers of observed events and the predicted background yields in the STA-STA category are shown in Fig. 10 in representative $m_{\mu\mu}$ and $m_{\mu\mu}^{\text{corr}}$ intervals. The width of the mass intervals and the $|\Delta\Phi|$ and $m_{\mu\mu}$ requirements for events in Fig. 10 (left) and Fig. 10 (right) correspond to those chosen, respectively, for the study of the HAHM and of the RPV SUSY model. For illustrative purposes, signal distributions at the level of the median expected exclusion limits at 95% confidence level (CL) obtained from the ensemble of both dimuon categories in the background-only scenario are also shown. The numbers of observed events are consistent with background predictions. As expected for background events, most of the observed events have low $m_{\mu\mu}$.

The numbers of observed events and the predicted background yields in the TMS-TMS category are shown in Figs. 11–13. Figure 11 shows the distributions of $\min(d_0/\sigma_{d_0})$ for TMS-TMS dimuons with (left) $|\Delta\Phi| < \pi/30$ and (right) $|\Delta\Phi| < \pi/4$, for events in all mass intervals combined. As expected for background events, the events in data are predominantly at low values of $\min(d_0/\sigma_{d_0})$. Figure 12 shows the distributions of $m_{\mu\mu}^{\text{corr}}$ in three $\min(d_0/\sigma_{d_0})$ bins, 6–10, 10–20, and >20, for dimuons with $|\Delta\Phi| < \pi/4$, the looser $|\Delta\Phi|$ requirement used for the study of the RPV SUSY model. The numbers of events in the SR chosen for the study of the HAHM model, with the tighter requirement $|\Delta\Phi| < \pi/30$, are smaller (with no more than one event per $m_{\mu\mu}$ bin), as shown in Fig. 13. The numbers of observed events are consistent with background predictions in both SRs. The largest $\min(d_0/\sigma_{d_0})$ bin, $\min(d_0/\sigma_{d_0}) > 20$, contains the lowest experimental background and, except for the smallest lifetimes, most of the signal predicted by both models.

These results are used to set upper limits on $\mathcal{B}(\mathrm{H} \to \mathrm{Z_D Z_D})$ in the HAHM model and on the product of the squark-antisquark production cross section $\sigma(\mathrm{pp} \to \tilde{\mathrm{q}}\bar{\tilde{\mathrm{q}}})$ and $\mathcal{B}(\tilde{\mathrm{q}} \to \mathrm{q}\tilde{\chi}_1^0)$ in the RPV SUSY model. The limit extraction is based on a modified frequentist approach [37, 38] and

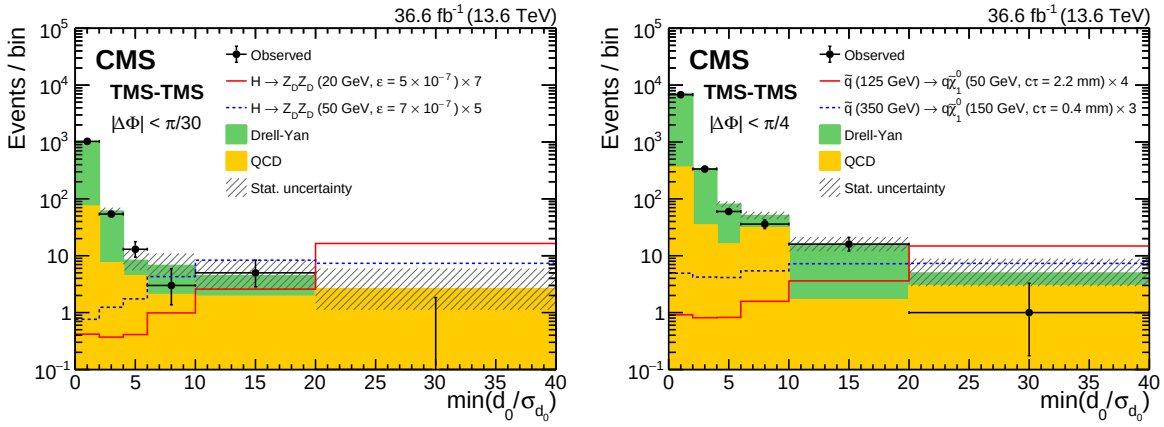

Figure 11: Distributions of $\min(d_0/\sigma_{d_0})$ for TMS-TMS dimuons with (left) $|\Delta\Phi| < \pi/30$ and (right) $|\Delta\Phi| < \pi/4$, for events in all mass intervals combined, for both the validation ($\min(d_0/\sigma_{d_0}) < 6$) and signal ($\min(d_0/\sigma_{d_0}) > 6$) regions. The number of observed events (black circles) is overlaid with the stacked histograms showing the expected numbers of QCD (yellow) and DY (green) background events. Statistical uncertainties in the total expected background are shown as hatched histograms. Signal contributions expected from simulated signals indicated in the legends are shown in red and blue. Their yields are set to the corresponding median expected 95% CL exclusion limits obtained from the ensemble of both dimuon categories, scaled up as indicated in the legend to improve visibility. Events are required to satisfy all nominal selection criteria with the exception of the d_0/σ_{d_0} requirement. The last bin includes events in the histogram overflow.

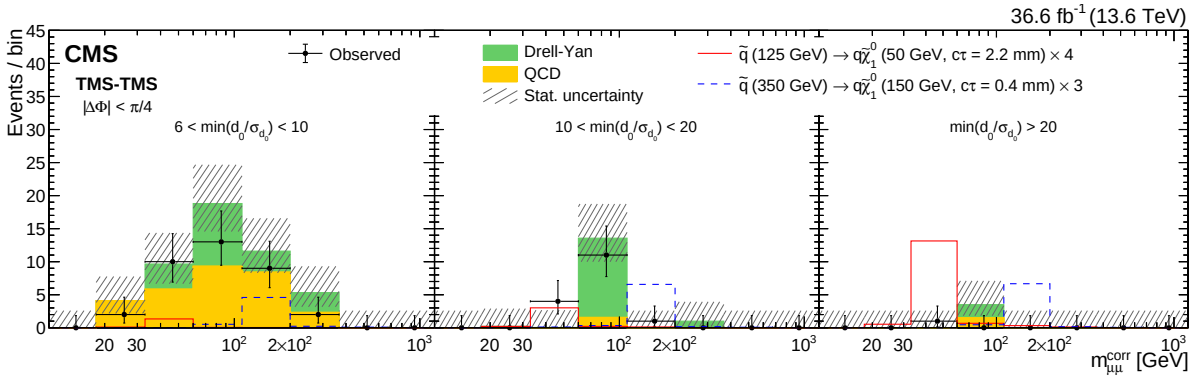

Figure 12: Comparison of observed and expected numbers of events in bins of $m_{\mu\mu}^{\text{corr}}$ in the TMS-TMS dimuon category, in the signal regions optimized for the RPV SUSY model. The number of observed events (black circles) is overlaid with the stacked filled histograms showing the expected numbers of QCD (yellow) and DY (green) background events in bins of $m_{\mu\mu}^{\text{corr}}$ in three $\min(d_0/\sigma_{d_0})$ bins: (left) 6–10, (center) 10–20, and (right) >20. Hatched histograms show statistical uncertainties in the total expected background. Contributions expected from signal events predicted by the RPV SUSY model with the parameters indicated in the legends are shown as red and blue histograms. Their yields are set to the corresponding median expected 95% CL exclusion limits obtained from the ensemble of both dimuon categories, scaled up as indicated in the legend to improve visibility. The last bin includes events in the histogram overflow.

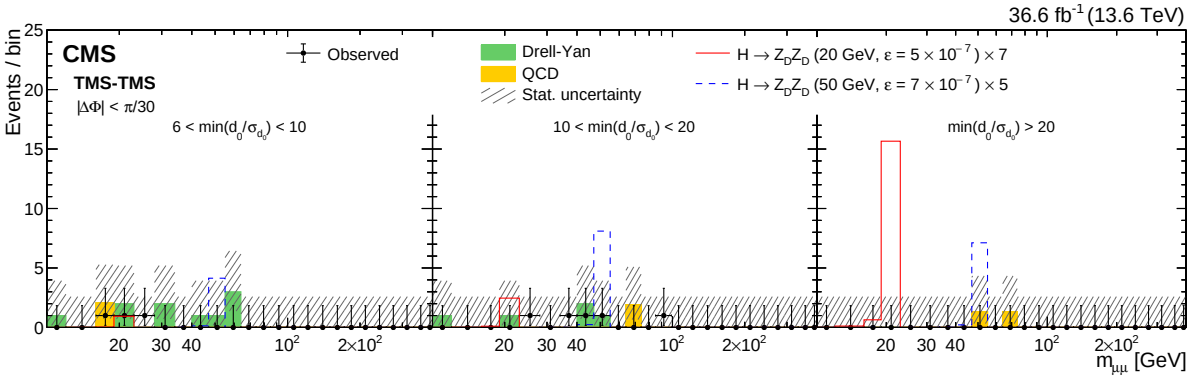

Figure 13: Comparison of observed and expected numbers of events in bins of $m_{\mu\mu}$ in the TMS-TMS dimuon category, in the signal regions optimized for the HAHM. The number of observed events (black circles) is overlaid with the stacked histograms showing the expected numbers of QCD (yellow) and DY (green) background events in bins of $m_{\mu\mu}$ in three $\min(d_0/\sigma_{d_0})$ bins: (left) 6–10, (center) 10–20, and (right) >20. Hatched histograms show statistical uncertainties in the total expected background. Signal contributions expected from simulated $H \to Z_D Z_D$ events with the parameters indicated in the legends are shown as red and blue histograms. Their yields are set to the corresponding median expected 95% CL exclusion limits obtained from the ensemble of both dimuon categories, scaled up as indicated in the legend to improve visibility. The last bin includes events in the histogram overflow.

uses the CMS statistical analysis tool COMBINE [39]. The method yielding background predictions in the SR is implemented using a multibin likelihood, which is a product of Poisson distributions corresponding to the SR and CRs. The systematic uncertainties affecting the signal yield are incorporated as nuisance parameters using log-normal distributions. The expected and observed upper limits are evaluated through the use of simulated pseudo-experiments. For each signal model, the limits are first computed separately in each dimuon category. The individual likelihoods are then combined to obtain the limits in the ensemble of both categories. For the interpretation in the framework of the HAHM model, the results obtained in this analysis are also combined with the results of the Run 2 analysis [5] to achieve even stronger bounds on the model parameters. The combination of the two results takes into account the different cross sections of the Higgs boson production in collisions at 13.0 and 13.6 TeV [20, 21].

The signal efficiencies used in the statistical interpretations of the results are obtained from simulation and further corrected by the data-to-simulation scale factors described in Section 6. They are computed separately for each dimuon category, mass interval, LLP lifetime, and signal model. Given the smallness of the expected background and taking into account the selection efficiencies discussed in Section 4, the introduction of a separate category for events with two dimuons would not increase the sensitivity of the analysis significantly even in the most favorable case for the 4μ signal events, namely $\mathcal{B}(\text{LLP} \to \mu^+\mu^-\text{X}) = 1$. The gain would be negligible for smaller $\mathcal{B}(\text{Z}_\text{D} \to \mu^+\mu^-)$ values predicted by the HAHM model. Therefore, no distinction is made between events with one and two reconstructed dimuons of the same type. Events with two TMS-TMS dimuons are assigned to the $\min(d_0/\sigma_{d_0})$ bin encompassing the larger of the two $\min(d_0/\sigma_{d_0})$ values.

Figures 14 and 15 show the 95% CL upper limits obtained in the framework of the HAHM model under the assumption that $m(\text{H}_\text{D}) > m(\text{H})/2$. The limits shown in these figures are set on $\mathcal{B}(\text{H} \to \text{Z}_\text{D}\text{Z}_\text{D})$ as functions of the mean proper decay length of Z_D for $m(\text{Z}_\text{D})$ in the range 10–60 GeV. Figure 14 shows the results obtained in this analysis, namely the expected limits in

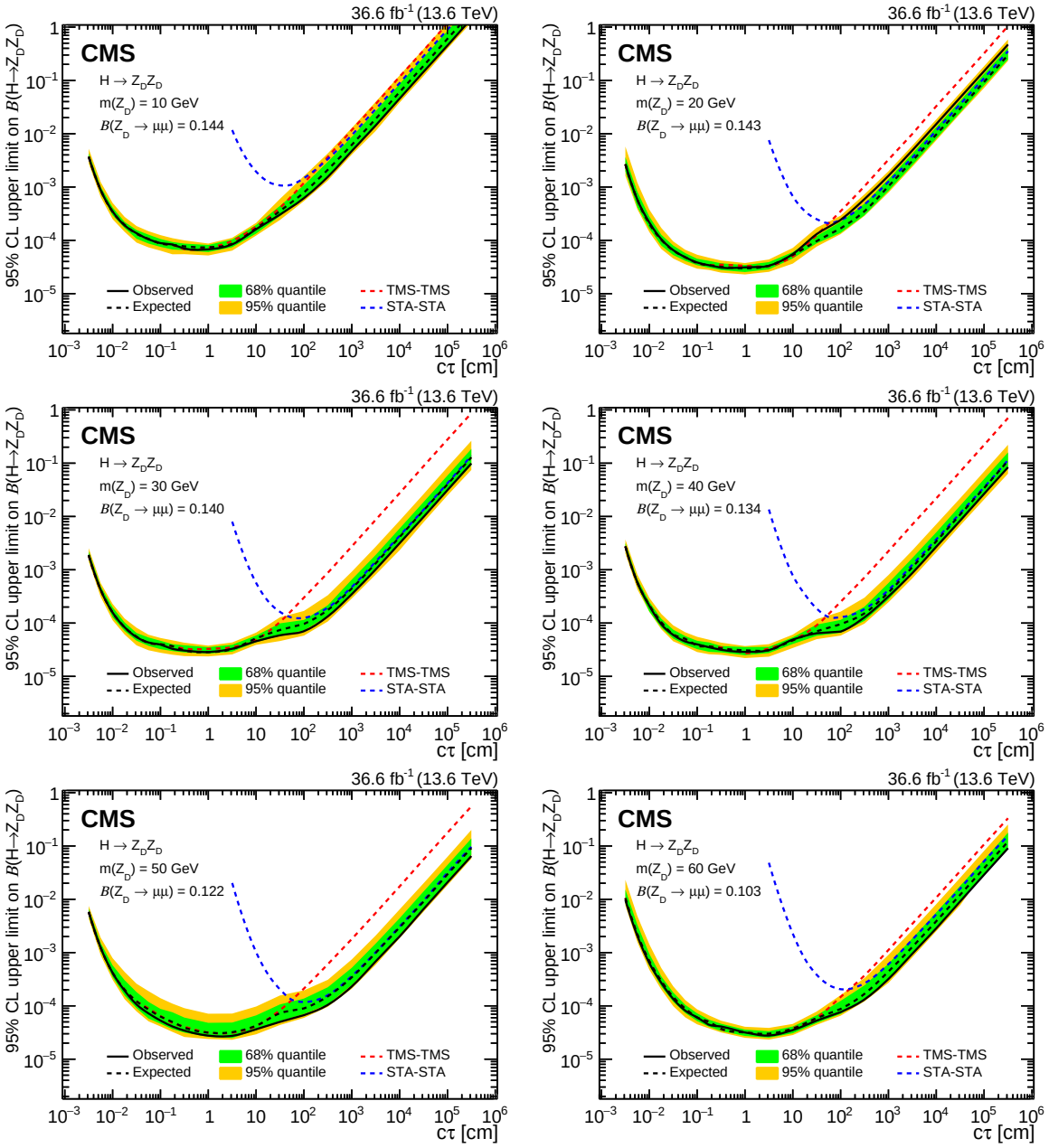

Figure 14: The 95% CL upper limits on $\mathcal{B}(\mathrm{H} \to \mathrm{Z_D Z_D})$ as a function of $c\tau(\mathrm{Z_D})$ in the HAHM model, for $m(\mathrm{Z_D})$ ranging from (upper left) 10 GeV to (lower right) 60 GeV, in the STA-STA and TMS-TMS dimuon categories in 2022 data and their combination. The median expected limits obtained from the STA-STA and TMS-TMS dimuon categories are shown as dashed blue and red curves, respectively; the combined median expected limits are shown as dashed black curves; and the combined observed limits are shown as solid black curves. The green and yellow bands correspond, respectively, to the 68 and 95% quantiles for the combined expected limits.

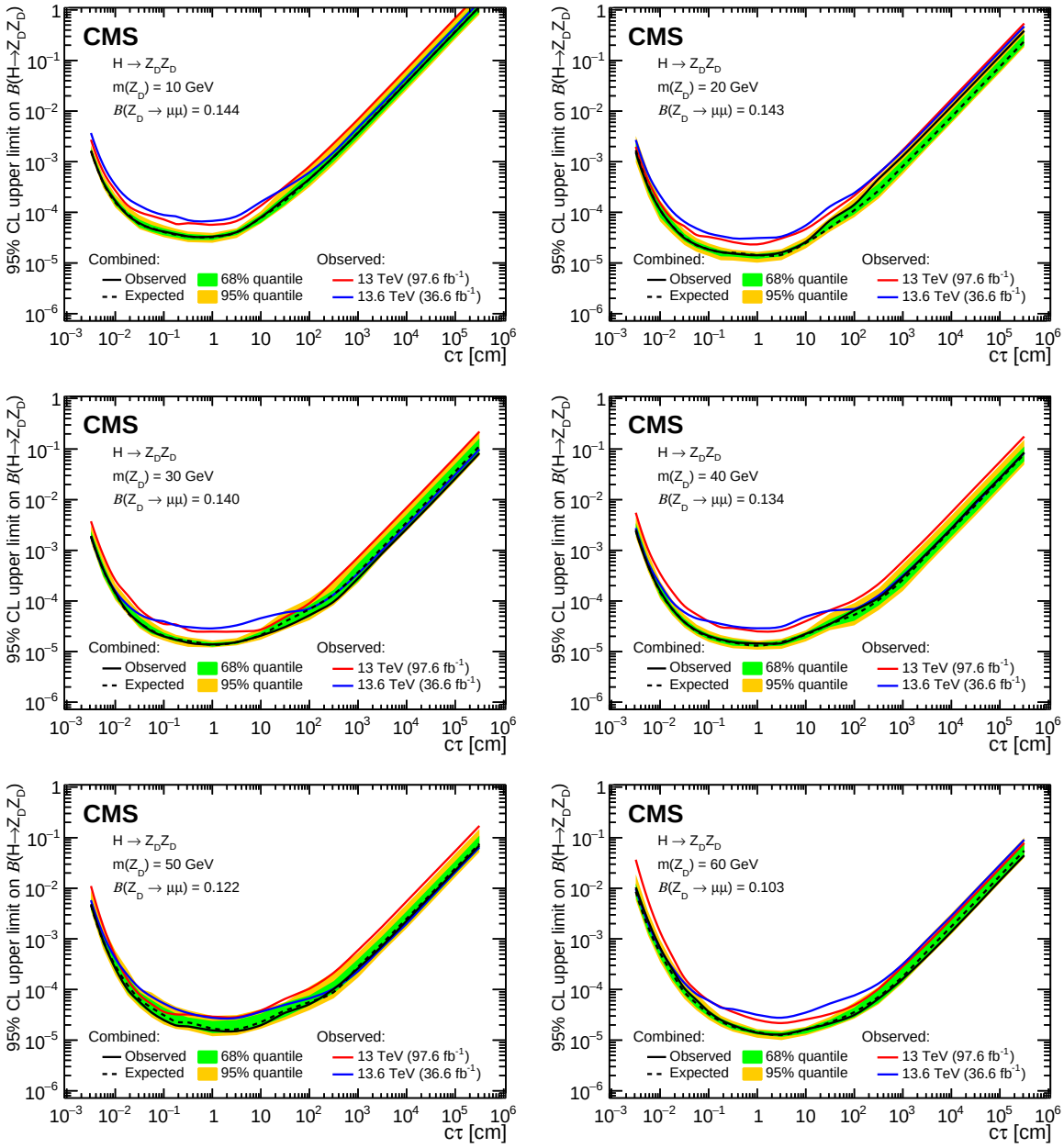

Figure 15: The 95% CL upper limits on $\mathcal{B}(\mathrm{H} \to \mathrm{Z_D Z_D})$ as a function of $c\tau(\mathrm{Z_D})$ in the HAHM model, for $m(\mathrm{Z_D})$ ranging from (upper left) 10 GeV to (lower right) 60 GeV, obtained in this analysis, the Run 2 analysis [5], and their combination. The observed limits in this analysis and in the Run 2 analysis [5] are shown as blue and red curves, respectively; the median combined expected limits are shown as dashed black curves; and the combined observed limits are shown as solid black curves. The green and yellow bands correspond, respectively, to the 68 and 95% quantiles for the combined expected limits.

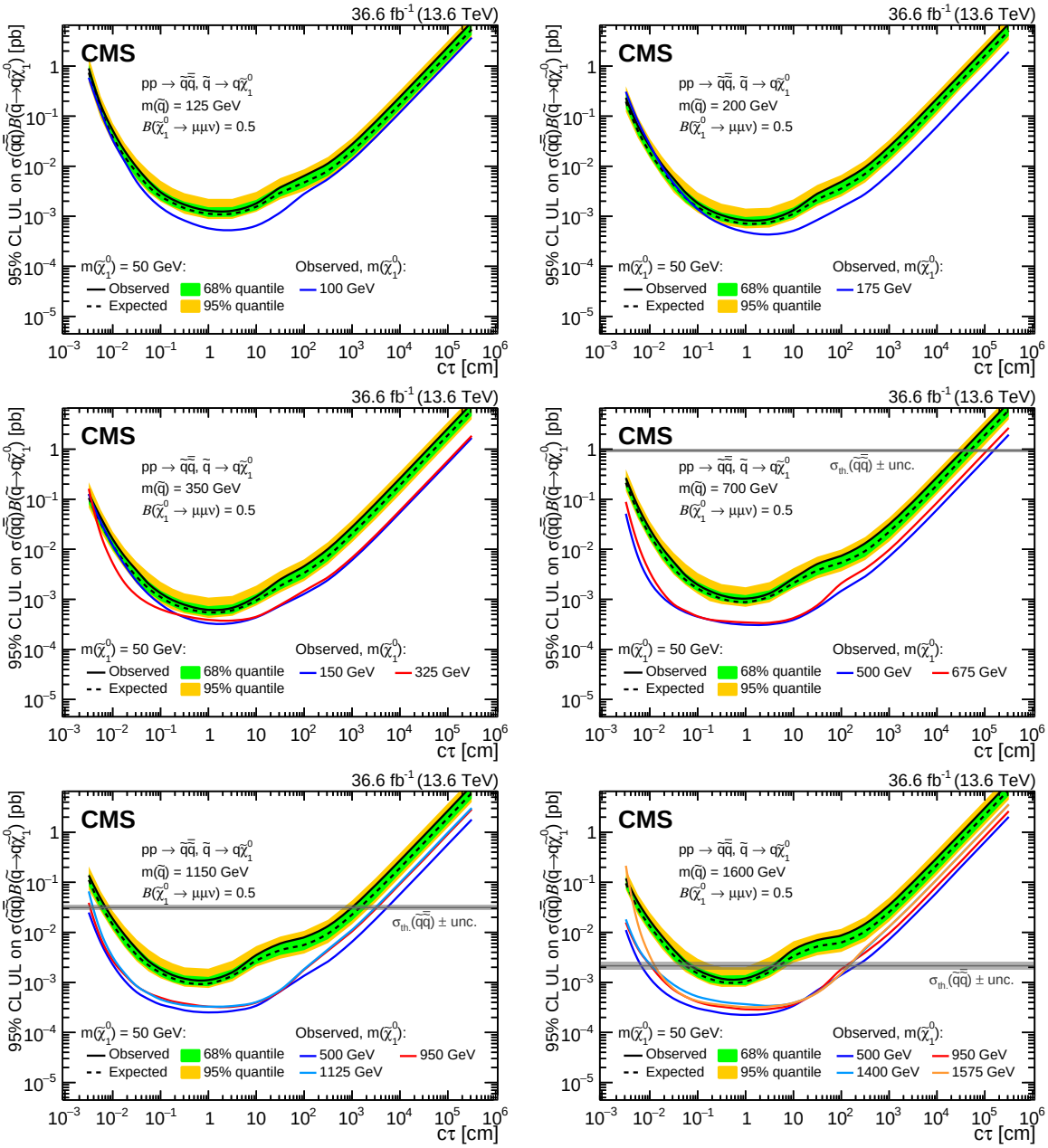

Figure 16: The 95% CL upper limits on $\sigma(\mathrm{pp} \to \tilde{\mathrm{q}}\bar{\tilde{\mathrm{q}}})\mathcal{B}(\tilde{\mathrm{q}} \to \mathrm{q}\tilde{\chi}_1^0)$ as a function of $c\tau(\tilde{\chi}_1^0)$ in the RPV SUSY model, for $\mathcal{B}(\tilde{\chi}_1^0 \to \mu^+\mu^-\nu) = 0.5$ and $m(\tilde{\mathrm{q}})$ ranging from (upper left) 125 GeV to (lower right) 1.6 TeV. The observed limits for various combinations of $m(\tilde{\mathrm{q}})$ and $m(\tilde{\chi}_1^0)$ indicated in the legends are shown as solid curves. The median expected limits and their 68 and 95% quantiles are shown, respectively, as dashed black curves and green and yellow bands for the case of $m(\tilde{\chi}_1^0) = 50$ GeV and omitted for other neutralino masses for clarity. The gray horizontal lines indicate the theoretical values of the squark-antisquark production cross sections with the uncertainties shown as gray shaded bands. The predicted cross sections for $m(\tilde{\mathrm{q}})$ = 125, 200, and 350 GeV are, respectively, 7200, 840, and 50 pb, and fall outside the y-axis range.

the individual dimuon categories as well as the expected and observed limits obtained in the ensemble of both categories. Figure 15 compares the observed limits obtained in this analysis with the corresponding Run 2 limits [5], and shows the expected and observed limits obtained in a combination of the two results.

Even though the size of the data sample used by this analysis is about a factor of 2.5 smaller than that in the Run 2 analysis, the constraints on the parameters of the HAHM model are comparable or tighter in a significant fraction of the parameter space, thanks mainly to improvements in the trigger algorithms. The combined limits on $\mathcal{B}(\mathrm{H} \to \mathrm{Z_D Z_D})$ are approximately a factor of 2 more stringent than the limits obtained in the Run 2 analysis. They exclude $\mathcal{B}(\mathrm{H} \to \mathrm{Z_D Z_D})$ of 1% in the range of $c\tau(\mathrm{Z_D})$ from a few tens of μm to 30 m (700 m) for $m(\mathrm{Z_D})$ = 10 GeV (60 GeV) at 95% CL. In the $m(\mathrm{Z_D})$ interval 20–60 GeV, $\mathcal{B}(\mathrm{H} \to \mathrm{Z_D Z_D})$ as low as 0.01% is excluded at 95% CL in the $c\tau(\mathrm{Z_D})$ range of about 0.3 mm to 0.5 m, which corresponds to a wide range of ϵ values from $\approx 10^{-8}$ to $\approx 10^{-6}$. These constraints on rare SM Higgs boson decays are tighter than those derived from searches for invisible Higgs boson decays [40, 41] and from measurements of the SM Higgs boson couplings [42]. At $m(\mathrm{Z_D}) > 20$ GeV, the limits obtained are the most stringent limits to date for all $c\tau(\mathrm{Z_D})$ values except those between $\approx$0.1 and $\approx$10 cm (depending on $m(\mathrm{Z_D})$), where a previous CMS search [7] using data collected with a dedicated high-rate data stream provides the best limits.

Figure 16 shows the observed and expected 95% CL upper limits obtained in the ensemble of both dimuon categories in the framework of the RPV SUSY model. The limits are set on the product $\sigma(\mathrm{pp} \to \tilde{\mathrm{q}}\bar{\tilde{\mathrm{q}}})\mathcal{B}(\tilde{\mathrm{q}} \to \mathrm{q}\tilde{\chi}_1^0)$ assuming $\mathcal{B}(\tilde{\chi}_1^0 \to \mu^+\mu^-\nu) = 0.5$. They are shown as functions of the mean proper decay length of $\tilde{\chi}_1^0$ for the various combinations of $m(\tilde{\mathrm{q}})$ and $m(\tilde{\chi}_1^0)$ indicated in the legends, for $m(\tilde{\mathrm{q}})$ values ranging from 125 GeV to 1.6 TeV, and compared to the theoretical predictions. At a squark mass of 700 GeV, the data exclude the mean proper neutralino decay lengths between 30 μm and 350 m (at $m(\tilde{\chi}_1^0) = 50$ GeV), and between 30 μm and 1.5 km (at $m(\tilde{\chi}_1^0) = 500$ GeV). At a squark mass of 1.6 TeV, the excluded $c\tau(\tilde{\chi}_1^0)$ range is between 0.07 and 4 cm for $m(\tilde{\chi}_1^0) = 50$ GeV and between 70 μm and 2 m for $m(\tilde{\chi}_1^0) = 500$ GeV. The limits obtained in this analysis are tighter than those derived by CMS in the Run 1 search [8, 9] in all of the relevant ($m(\tilde{\mathrm{q}})$, $m(\tilde{\chi}_1^0)$, $c\tau(\tilde{\chi}_1^0)$) parameter space and are more stringent at $c\tau(\tilde{\chi}_1^0) \lesssim 1$ cm and $c\tau(\tilde{\chi}_1^0) \gtrsim 1$ m than the limits on the λ_{122} RPV coupling set by the ATLAS Collaboration at $m(\tilde{\mathrm{q}})$ of 700 GeV and 1.6 TeV [11].

8 Summary

Data collected by the CMS experiment in proton-proton collisions at $\sqrt{s} = 13.6$ TeV in 2022 and corresponding to an integrated luminosity of 36.6 fb^{-1} have been used to conduct an inclusive search for long-lived exotic neutral particles decaying to final states with a pair of oppositely charged muons. The search strategy is largely model independent and is sensitive to a broad range of lifetimes and masses. No significant excess of events above the standard model background is observed. The results are interpreted as limits on the parameters of the hidden Abelian Higgs model, in which the Higgs boson H decays to a pair of long-lived dark photons $\mathrm{Z_D}$, and of an R-parity violating supersymmetry model, in which long-lived neutralinos decay to a pair of muons and a neutrino.

Even though the size of the data sample used by this analysis is about a factor of 2.5 smaller than that used in the previous search for displaced dimuons by the CMS experiment in pp collisions at $\sqrt{s} = 13$ TeV, the constraints on the parameters of the hidden Abelian Higgs model are comparable or tighter in a significant fraction of the parameter space, thanks mainly to

improvements in the trigger algorithms. The combination of the results of this analysis with the results obtained at $\sqrt{s} = 13\,\text{TeV}$ improves the constraints on the branching fraction of the Higgs boson to dark photons, $\mathcal{B}(\text{H} \to \text{Z}_\text{D}\text{Z}_\text{D})$, by approximately a factor of 2. In the range 10–60 GeV of the Z_D mass $m(\text{Z}_\text{D})$, $\mathcal{B}(\text{H} \to \text{Z}_\text{D}\text{Z}_\text{D}) = 1\%$ is excluded at 95% confidence level in the range of proper decay length $c\tau(\text{Z}_\text{D})$ from a few tens of μm to 30 m (700 m) for $m(\text{Z}_\text{D})$ = 10 GeV (60 GeV). For $m(\text{Z}_\text{D})$ greater than 20 GeV and less than $m(\text{H})/2$, the combined limits provide the most stringent constraints to date on $\mathcal{B}(\text{H} \to \text{Z}_\text{D}\text{Z}_\text{D})$ for $c\tau(\text{Z}_\text{D})$ between 30 μm and $\approx$0.1 cm, and above $\approx$10 cm. When interpreted in the framework of the R-parity violating supersymmetry model at a squark mass of 1.6 TeV, the results exclude mean proper neutralino decay lengths between 0.07 and 4 cm for a 50 GeV neutralino and between 70 μm and 2 m for a 500 GeV neutralino.

Acknowledgments

We congratulate our colleagues in the CERN accelerator departments for the excellent performance of the LHC and thank the technical and administrative staffs at CERN and at other CMS institutes for their contributions to the success of the CMS effort. In addition, we gratefully acknowledge the computing centers and personnel of the Worldwide LHC Computing Grid and other centers for delivering so effectively the computing infrastructure essential to our analyses. Finally, we acknowledge the enduring support for the construction and operation of the LHC, the CMS detector, and the supporting computing infrastructure provided by the following funding agencies: SC (Armenia), BMBWF and FWF (Austria); FNRS and FWO (Belgium); CNPq, CAPES, FAPERJ, FAPERGS, and FAPESP (Brazil); MES and BNSF (Bulgaria); CERN; CAS, MoST, and NSFC (China); MINCIENCIAS (Colombia); MSES and CSF (Croatia); RIF (Cyprus); SENESCYT (Ecuador); ERC PRG, RVTT3 and MoER TK202 (Estonia); Academy of Finland, MEC, and HIP (Finland); CEA and CNRS/IN2P3 (France); SRNSF (Georgia); BMBF, DFG, and HGF (Germany); GSRI (Greece); NKFIH (Hungary); DAE and DST (India); IPM (Iran); SFI (Ireland); INFN (Italy); MSIP and NRF (Republic of Korea); MES (Latvia); LMTLT (Lithuania); MOE and UM (Malaysia); BUAP, CINVESTAV, CONACYT, LNS, SEP, and UASLP-FAI (Mexico); MOS (Montenegro); MBIE (New Zealand); PAEC (Pakistan); MES and NSC (Poland); FCT (Portugal); MESTD (Serbia); MCIN/AEI and PCTI (Spain); MOSTR (Sri Lanka); Swiss Funding Agencies (Switzerland); MST (Taipei); MHESI and NSTDA (Thailand); TUBITAK and TENMAK (Turkey); NASU (Ukraine); STFC (United Kingdom); DOE and NSF (USA).

Individuals have received support from the Marie-Curie program and the European Research Council and Horizon 2020 Grant, contract Nos. 675440, 724704, 752730, 758316, 765710, 824093, 101115353, and COST Action CA16108 (European Union); the Leventis Foundation; the Alfred P. Sloan Foundation; the Alexander von Humboldt Foundation; the Science Committee, project no. 22rl-037 (Armenia); the Belgian Federal Science Policy Office; the Fonds pour la Formation à la Recherche dans l'Industrie et dans l'Agriculture (FRIA-Belgium); the Agentschap voor Innovatie door Wetenschap en Technologie (IWT-Belgium); the F.R.S.-FNRS and FWO (Belgium) under the "Excellence of Science – EOS" – be.h project n. 30820817; the Beijing Municipal Science & Technology Commission, No. Z191100007219010 and Fundamental Research Funds for the Central Universities (China); the Ministry of Education, Youth and Sports (MEYS) of the Czech Republic; the Shota Rustaveli National Science Foundation, grant FR-22-985 (Georgia); the Deutsche Forschungsgemeinschaft (DFG), under Germany's Excellence Strategy – EXC 2121 "Quantum Universe" – 390833306, and under project number 400140256 - GRK2497; the Hellenic Foundation for Research and Innovation (HFRI), Project Number 2288 (Greece); the Hungarian Academy of Sciences, the New National Excellence Program - ÚNKP,

the NKFIH research grants K 124845, K 124850, K 128713, K 128786, K 129058, K 131991, K 133046, K 138136, K 143460, K 143477, 2020-2.2.1-ED-2021-00181, and TKP2021-NKTA-64 (Hungary); the Council of Science and Industrial Research, India; ICSC – National Research Center for High Performance Computing, Big Data and Quantum Computing, funded by the NextGenerationEU program (Italy); the Latvian Council of Science; the Ministry of Education and Science, project no. 2022/WK/14, and the National Science Center, contracts Opus 2021/41/B/ST2/01369 and 2021/43/B/ST2/01552 (Poland); the Fundação para a Ciência e a Tecnologia, grant CEECIND/01334/2018 (Portugal); the National Priorities Research Program by Qatar National Research Fund; MCIN/AEI/10.13039/501100011033, ERDF "a way of making Europe", and the Programa Estatal de Fomento de la Investigación Científica y Técnica de Excelencia María de Maeztu, grant MDM-2017-0765 and Programa Severo Ochoa del Principado de Asturias (Spain); the Chulalongkorn Academic into Its 2nd Century Project Advancement Project, and the National Science, Research and Innovation Fund via the Program Management Unit for Human Resources & Institutional Development, Research and Innovation, grant B37G660013 (Thailand); the Kavli Foundation; the Nvidia Corporation; the SuperMicro Corporation; the Welch Foundation, contract C-1845; and the Weston Havens Foundation (USA).

References

[1] J. L. Hewett, B. Lillie, M. Masip, and T. G. Rizzo, "Signatures of long-lived gluinos in split supersymmetry", *JHEP* **09** (2004) 070, doi:10.1088/1126-6708/2004/09/070, arXiv:hep-ph/0408248.

[2] R. Barbier et al., "*R*-parity-violating supersymmetry", *Phys. Rept.* **420** (2005) 1, doi:10.1016/j.physrep.2005.08.006, arXiv:hep-ph/0406039.

[3] M. J. Strassler and K. M. Zurek, "Echoes of a hidden valley at hadron colliders", *Phys. Lett. B* **651** (2007) 374, doi:10.1016/j.physletb.2007.06.055, arXiv:hep-ph/0604261.

[4] T. Han, Z. Si, K. M. Zurek, and M. J. Strassler, "Phenomenology of hidden valleys at hadron colliders", *JHEP* **07** (2008) 008, doi:10.1088/1126-6708/2008/07/008, arXiv:0712.2041.

[5] CMS Collaboration, "Search for long-lived particles decaying to a pair of muons in proton-proton collisions at $\sqrt{s} = 13\,\text{TeV}$", *JHEP* **05** (2023) 228, doi:10.1007/JHEP05(2023)228, arXiv:2205.08582.

[6] D. Curtin, R. Essig, S. Gori, and J. Shelton, "Illuminating dark photons with high-energy colliders", *JHEP* **02** (2015) 157, doi:10.1007/JHEP02(2015)157, arXiv:1412.0018.

[7] CMS Collaboration, "Search for long-lived particles decaying into muon pairs in proton-proton collisions at $\sqrt{s} = 13\,\text{TeV}$ collected with a dedicated high-rate data stream", *JHEP* **04** (2022) 062, doi:10.1007/JHEP04(2022)062, arXiv:2112.13769.

[8] CMS Collaboration, "Search for long-lived particles that decay into final states containing two electrons or two muons in proton-proton collisions at $\sqrt{s} = 8\,\text{TeV}$", *Phys. Rev. D* **91** (2015) 052012, doi:10.1103/PhysRevD.91.052012, arXiv:1411.6977.

[9] CMS Collaboration, "Search for long-lived particles that decay into final states containing two muons, reconstructed using only the CMS muon chambers", CMS Physics Analysis Summary CMS-PAS-EXO-14-012, 2015.

[10] ATLAS Collaboration, "Search for long-lived particles in final states with displaced dimuon vertices in pp collisions at $\sqrt{s} = 13$ TeV with the ATLAS detector", *Phys. Rev. D* **99** (2019) 012001, doi:10.1103/PhysRevD.99.012001, arXiv:1808.03057.

[11] ATLAS Collaboration, "Search for displaced vertices of oppositely charged leptons from decays of long-lived particles in pp collisions at $\sqrt{s} = 13$ TeV with the ATLAS detector", *Phys. Lett. B* **801** (2020) 135114, doi:10.1016/j.physletb.2019.135114, arXiv:1907.10037.

[12] HEPData record for this analysis, 2024. doi:10.17182/hepdata.146759.

[13] CMS Collaboration, "Performance of the CMS muon detector and muon reconstruction with proton-proton collisions at $\sqrt{s} = 13$ TeV", *JINST* **13** (2018) P06015, doi:10.1088/1748-0221/13/06/P06015, arXiv:1804.04528.

[14] CMS Collaboration, "The CMS experiment at the CERN LHC", *JINST* **3** (2008) S08004, doi:10.1088/1748-0221/3/08/S08004.

[15] CMS Collaboration, "Development of the CMS detector for the CERN LHC Run 3", 2023. arXiv:2309.05466. Accepted by *JINST*.

[16] CMS Collaboration, "Performance of the CMS Level-1 trigger in proton-proton collisions at $\sqrt{s} = 13$ TeV", *JINST* **15** (2020) P10017, doi:10.1088/1748-0221/15/10/P10017, arXiv:2006.10165.

[17] CMS Collaboration, "The CMS trigger system", *JINST* **12** (2017) P01020, doi:10.1088/1748-0221/12/01/P01020, arXiv:1609.02366.

[18] J. D. Wells, "How to find a hidden world at the Large Hadron Collider", in *Perspectives on LHC Physics*, G. Kane and A. Pierce, eds., p. 283. World Scientific, Singapore, 2008. arXiv:0803.1243. doi:10.1142/9789812779762_0015.

[19] J. Alwall et al., "The automated computation of tree-level and next-to-leading order differential cross sections, and their matching to parton shower simulations", *JHEP* **07** (2014) 079, doi:10.1007/JHEP07(2014)079, arXiv:1405.0301.

[20] M. Cepeda et al., "Report from working group 2: Higgs physics at the HL-LHC and HE-LHC", in *Proceedings of the HL/HE-LHC Workshop*, A. Dainese et al., eds., volume 7, p. 221. 2019. arXiv:1902.00134. CERN Yellow Rep. Monogr. doi:10.23731/CYRM-2019-007.221.

[21] LHC Higgs Cross Section Working Group, "Ad interim 13.6 TeV cross sections", 2023. https://twiki.cern.ch/twiki/bin/view/LHCPhysics/LHCHWG136TeVxsec_extrap.

[22] T. Sjöstrand et al., "An introduction to PYTHIA 8.2", *Comput. Phys. Commun.* **191** (2015) 159, doi:10.1016/j.cpc.2015.01.024, arXiv:1410.3012.

[23] H. K. Dreiner, "An introduction to explicit R-parity violation", *Adv. Ser. Direct. High Energy Phys.* **21** (2010) 565, doi:10.1142/9789814307505_0017, arXiv:hep-ph/9707435.

[24] D. Dercks et al., "R-parity violation at the LHC", *Eur. Phys. J. C* **77** (2017) 856, doi:10.1140/epjc/s10052-017-5414-4, arXiv:1706.09418.

[25] W. Beenakker et al., "NNLL-fast: predictions for coloured supersymmetric particle production at the LHC with threshold and Coulomb resummation", *JHEP* **12** (2016) 133, doi:10.1007/JHEP12(2016)133, arXiv:1607.07741.

[26] PDF4LHC Working Group, R. D. Ball et al., "The PDF4LHC21 combination of global PDF fits for the LHC Run III", *J. Phys. G* **49** (2022) 080501, doi:10.1088/1361-6471/ac7216, arXiv:2203.05506.

[27] NNPDF Collaboration, "Parton distributions from high-precision collider data", *Eur. Phys. J. C* **77** (2017) 663, doi:10.1140/epjc/s10052-017-5199-5, arXiv:1706.00428.

[28] CMS Collaboration, "Extraction and validation of a new set of CMS PYTHIA8 tunes from underlying-event measurements", *Eur. Phys. J. C* **80** (2020) 4, doi:10.1140/epjc/s10052-019-7499-4, arXiv:1903.12179.

[29] GEANT4 Collaboration, "GEANT4—a simulation toolkit", *Nucl. Instrum. Meth. A* **506** (2003) 250, doi:10.1016/S0168-9002(03)01368-8.

[30] W. A. Nash, "Search for long-lived particles that decay to muon pairs at 13 TeV and an algorithm to improve resolution in the muon system of the Compact Muon Solenoid". PhD thesis, University of California, Los Angeles, 2022. https://escholarship.org/uc/item/3gw9h84p.

[31] CMS Collaboration, "Technical proposal for the Phase-II upgrade of the Compact Muon Solenoid", CMS Technical Proposal CERN-LHCC-2015-010, CMS-TDR-15-02, 2015.

[32] CMS Collaboration, "Performance of the CMS muon trigger system in proton-proton collisions at $\sqrt{s} = 13$ TeV", *JINST* **16** (2021) P07001, doi:10.1088/1748-0221/16/07/P07001, arXiv:2102.04790.

[33] CMS Collaboration, "Performance of CMS muon reconstruction in pp collision events at $\sqrt{s} = 7$ TeV", *JINST* **7** (2012) P10002, doi:10.1088/1748-0221/7/10/P10002, arXiv:1206.4071.

[34] LHCb Collaboration, "Identification of beauty and charm quark jets at LHCb", *JINST* **10** (2015) P06013, doi:10.1088/1748-0221/10/06/P06013, arXiv:1504.07670.

[35] CMS Collaboration, "Identification of heavy-flavour jets with the CMS detector in pp collisions at 13 TeV", *JINST* **13** (2018) P05011, doi:10.1088/1748-0221/13/05/P05011, arXiv:1712.07158.

[36] CMS Collaboration, "First measurement of the top quark pair production cross section in proton-proton collisions at $\sqrt{s} = 13.6$ TeV", *JHEP* **08** (2023) 204, doi:10.1007/JHEP08(2023)204, arXiv:2303.10680.

[37] A. L. Read, "Presentation of search results: The CL_s technique", *J. Phys. G* **28** (2002) 2693, doi:10.1088/0954-3899/28/10/313.

[38] T. Junk, "Confidence level computation for combining searches with small statistics", *Nucl. Instrum. Meth. A* **434** (1999) 435, doi:10.1016/S0168-9002(99)00498-2, arXiv:hep-ex/9902006.

[39] CMS Collaboration, "The CMS statistical analysis and combination tool: COMBINE", 2024. arXiv:2404.06614. Submitted to *Comput. Softw. Big Sci.*

[40] CMS Collaboration, "A search for decays of the Higgs boson to invisible particles in events with a top-antitop quark pair or a vector boson in proton-proton collisions at $\sqrt{s} = 13\,\text{TeV}$", *Eur. Phys. J. C* **83** (2023) 933, doi:10.1140/epjc/s10052-023-11952-7, arXiv:2303.01214.

[41] CMS Collaboration, "Search for invisible decays of a Higgs boson produced through vector boson fusion in proton–proton collisions at $\sqrt{s} = 13\,\text{TeV}$", *Phys. Rev. D* **105** (2022) 092007, doi:10.1103/PhysRevD.105.092007, arXiv:2201.11585.

[42] CMS Collaboration, "Combined measurements of Higgs boson couplings in proton–proton collisions at $\sqrt{s} = 13\,\text{TeV}$", *Eur. Phys. J. C* **79** (2019) 421, doi:10.1140/epjc/s10052-019-6909-y, arXiv:1809.10733.

A The CMS Collaboration

Yerevan Physics Institute, Yerevan, Armenia
A. Hayrapetyan, A. Tumasyan[1]

Institut für Hochenergiephysik, Vienna, Austria
W. Adam, J.W. Andrejkovic, T. Bergauer, S. Chatterjee, K. Damanakis, M. Dragicevic, P.S. Hussain, M. Jeitler[2], N. Krammer, A. Li, D. Liko, I. Mikulec, J. Schieck[2], R. Schöfbeck, D. Schwarz, M. Sonawane, S. Templ, W. Waltenberger, C.-E. Wulz[2]

Universiteit Antwerpen, Antwerpen, Belgium
M.R. Darwish[3], T. Janssen, P. Van Mechelen

Vrije Universiteit Brussel, Brussel, Belgium
E.S. Bols, J. D'Hondt, S. Dansana, A. De Moor, M. Delcourt, S. Lowette, I. Makarenko, D. Müller, S. Tavernier, M. Tytgat[4], G.P. Van Onsem, S. Van Putte, D. Vannerom

Université Libre de Bruxelles, Bruxelles, Belgium
B. Clerbaux, A.K. Das, G. De Lentdecker, H. Evard, L. Favart, P. Gianneios, D. Hohov, J. Jaramillo, A. Khalilzadeh, F.A. Khan, K. Lee, M. Mahdavikhorrami, A. Malara, S. Paredes, L. Thomas, M. Vanden Bemden, C. Vander Velde, P. Vanlaer

Ghent University, Ghent, Belgium
M. De Coen, D. Dobur, Y. Hong, J. Knolle, L. Lambrecht, G. Mestdach, K. Mota Amarilo, C. Rendón, A. Samalan, K. Skovpen, N. Van Den Bossche, J. van der Linden, L. Wezenbeek

Université Catholique de Louvain, Louvain-la-Neuve, Belgium
A. Benecke, A. Bethani, G. Bruno, C. Caputo, C. Delaere, I.S. Donertas, A. Giammanco, Sa. Jain, V. Lemaitre, J. Lidrych, P. Mastrapasqua, T.T. Tran, S. Wertz

Centro Brasileiro de Pesquisas Fisicas, Rio de Janeiro, Brazil
G.A. Alves, E. Coelho, C. Hensel, T. Menezes De Oliveira, A. Moraes, P. Rebello Teles, M. Soeiro

Universidade do Estado do Rio de Janeiro, Rio de Janeiro, Brazil
W.L. Aldá Júnior, M. Alves Gallo Pereira, M. Barroso Ferreira Filho, H. Brandao Malbouisson, W. Carvalho, J. Chinellato[5], E.M. Da Costa, G.G. Da Silveira[6], D. De Jesus Damiao, S. Fonseca De Souza, R. Gomes De Souza, J. Martins[7], C. Mora Herrera, L. Mundim, H. Nogima, J.P. Pinheiro, A. Santoro, A. Sznajder, M. Thiel, A. Vilela Pereira

Universidade Estadual Paulista, Universidade Federal do ABC, São Paulo, Brazil
C.A. Bernardes[6], L. Calligaris, T.R. Fernandez Perez Tomei, E.M. Gregores, P.G. Mercadante, S.F. Novaes, B. Orzari, Sandra S. Padula

Institute for Nuclear Research and Nuclear Energy, Bulgarian Academy of Sciences, Sofia, Bulgaria
A. Aleksandrov, G. Antchev, R. Hadjiiska, P. Iaydjiev, M. Misheva, M. Shopova, G. Sultanov

University of Sofia, Sofia, Bulgaria
A. Dimitrov, L. Litov, B. Pavlov, P. Petkov, A. Petrov, E. Shumka

Instituto De Alta Investigación, Universidad de Tarapacá, Casilla 7 D, Arica, Chile
S. Keshri, S. Thakur

Beihang University, Beijing, China
T. Cheng, T. Javaid, L. Yuan

Department of Physics, Tsinghua University, Beijing, China
Z. Hu, J. Liu, K. Yi[8,9]

Institute of High Energy Physics, Beijing, China
G.M. Chen[10], H.S. Chen[10], M. Chen[10], F. Iemmi, C.H. Jiang, A. Kapoor[11], H. Liao, Z.-A. Liu[12], R. Sharma[13], J.N. Song[12], J. Tao, C. Wang[10], J. Wang, Z. Wang[10], H. Zhang

State Key Laboratory of Nuclear Physics and Technology, Peking University, Beijing, China
A. Agapitos, Y. Ban, A. Levin, C. Li, Q. Li, Y. Mao, S.J. Qian, X. Sun, D. Wang, H. Yang, L. Zhang, C. Zhou

Sun Yat-Sen University, Guangzhou, China
Z. You

University of Science and Technology of China, Hefei, China
K. Jaffel, N. Lu

Nanjing Normal University, Nanjing, China
G. Bauer[14]

Institute of Modern Physics and Key Laboratory of Nuclear Physics and Ion-beam Application (MOE) - Fudan University, Shanghai, China
X. Gao[15]

Zhejiang University, Hangzhou, Zhejiang, China
Z. Lin, C. Lu, M. Xiao

Universidad de Los Andes, Bogota, Colombia
C. Avila, D.A. Barbosa Trujillo, A. Cabrera, C. Florez, J. Fraga, J.A. Reyes Vega

Universidad de Antioquia, Medellin, Colombia
J. Mejia Guisao, F. Ramirez, M. Rodriguez, J.D. Ruiz Alvarez

University of Split, Faculty of Electrical Engineering, Mechanical Engineering and Naval Architecture, Split, Croatia
D. Giljanovic, N. Godinovic, D. Lelas, A. Sculac

University of Split, Faculty of Science, Split, Croatia
M. Kovac, T. Sculac

Institute Rudjer Boskovic, Zagreb, Croatia
P. Bargassa, V. Brigljevic, B.K. Chitroda, D. Ferencek, K. Jakovcic, S. Mishra, A. Starodumov[16], T. Susa

University of Cyprus, Nicosia, Cyprus
A. Attikis, K. Christoforou, A. Hadjiagapiou, S. Konstantinou, J. Mousa, C. Nicolaou, F. Ptochos, P.A. Razis, H. Rykaczewski, H. Saka, A. Stepennov

Charles University, Prague, Czech Republic
M. Finger, M. Finger Jr., A. Kveton

Escuela Politecnica Nacional, Quito, Ecuador
E. Ayala

Universidad San Francisco de Quito, Quito, Ecuador
E. Carrera Jarrin

Academy of Scientific Research and Technology of the Arab Republic of Egypt, Egyptian Network of High Energy Physics, Cairo, Egypt
H. Abdalla[17], Y. Assran[18,19]

Center for High Energy Physics (CHEP-FU), Fayoum University, El-Fayoum, Egypt
M.A. Mahmoud, Y. Mohammed

National Institute of Chemical Physics and Biophysics, Tallinn, Estonia
K. Ehataht, M. Kadastik, T. Lange, S. Nandan, C. Nielsen, J. Pata, M. Raidal, L. Tani, C. Veelken

Department of Physics, University of Helsinki, Helsinki, Finland
H. Kirschenmann, K. Osterberg, M. Voutilainen

Helsinki Institute of Physics, Helsinki, Finland
S. Bharthuar, E. Brücken, F. Garcia, K.T.S. Kallonen, R. Kinnunen, T. Lampén, K. Lassila-Perini, S. Lehti, T. Lindén, L. Martikainen, M. Myllymäki, M.m. Rantanen, H. Siikonen, E. Tuominen, J. Tuominiemi

Lappeenranta-Lahti University of Technology, Lappeenranta, Finland
P. Luukka, H. Petrow

IRFU, CEA, Université Paris-Saclay, Gif-sur-Yvette, France
M. Besancon, F. Couderc, M. Dejardin, D. Denegri, J.L. Faure, F. Ferri, S. Ganjour, P. Gras, G. Hamel de Monchenault, V. Lohezic, J. Malcles, L. Portales, J. Rander, A. Rosowsky, M.Ö. Sahin, A. Savoy-Navarro[20], P. Simkina, M. Titov, M. Tornago

Laboratoire Leprince-Ringuet, CNRS/IN2P3, Ecole Polytechnique, Institut Polytechnique de Paris, Palaiseau, France
F. Beaudette, A. Buchot Perraguin, P. Busson, A. Cappati, C. Charlot, M. Chiusi, F. Damas, O. Davignon, A. De Wit, I.T. Ehle, B.A. Fontana Santos Alves, S. Ghosh, A. Gilbert, R. Granier de Cassagnac, A. Hakimi, B. Harikrishnan, L. Kalipoliti, G. Liu, J. Motta, M. Nguyen, C. Ochando, R. Salerno, J.B. Sauvan, Y. Sirois, A. Tarabini, E. Vernazza, A. Zabi, A. Zghiche

Université de Strasbourg, CNRS, IPHC UMR 7178, Strasbourg, France
J.-L. Agram[21], J. Andrea, D. Apparu, D. Bloch, J.-M. Brom, E.C. Chabert, C. Collard, S. Falke, U. Goerlach, C. Grimault, R. Haeberle, A.-C. Le Bihan, M. Meena, G. Saha, M.A. Sessini, P. Van Hove

Institut de Physique des 2 Infinis de Lyon (IP2I), Villeurbanne, France
S. Beauceron, B. Blancon, G. Boudoul, N. Chanon, J. Choi, D. Contardo, P. Depasse, C. Dozen[22], H. El Mamouni, J. Fay, S. Gascon, M. Gouzevitch, C. Greenberg, G. Grenier, B. Ille, I.B. Laktineh, M. Lethuillier, L. Mirabito, S. Perries, A. Purohit, M. Vander Donckt, P. Verdier, J. Xiao

Georgian Technical University, Tbilisi, Georgia

I. Lomidze, T. Toriashvili[23], Z. Tsamalaidze[16]

RWTH Aachen University, I. Physikalisches Institut, Aachen, Germany
V. Botta, L. Feld, K. Klein, M. Lipinski, D. Meuser, A. Pauls, N. Röwert, M. Teroerde

RWTH Aachen University, III. Physikalisches Institut A, Aachen, Germany
S. Diekmann, A. Dodonova, N. Eich, D. Eliseev, F. Engelke, J. Erdmann, M. Erdmann, P. Fackeldey, B. Fischer, T. Hebbeker, K. Hoepfner, F. Ivone, A. Jung, M.y. Lee, F. Mausolf, M. Merschmeyer, A. Meyer, S. Mukherjee, D. Noll, F. Nowotny, A. Pozdnyakov, Y. Rath, W. Redjeb, F. Rehm, H. Reithler, U. Sarkar, V. Sarkisovi, A. Schmidt, A. Sharma, J.L. Spah, A. Stein, F. Torres Da Silva De Araujo[24], S. Wiedenbeck, S. Zaleski

RWTH Aachen University, III. Physikalisches Institut B, Aachen, Germany
C. Dziwok, G. Flügge, W. Haj Ahmad[25], T. Kress, A. Nowack, O. Pooth, A. Stahl, T. Ziemons, A. Zotz

Deutsches Elektronen-Synchrotron, Hamburg, Germany
H. Aarup Petersen, M. Aldaya Martin, J. Alimena, S. Amoroso, Y. An, S. Baxter, M. Bayatmakou, H. Becerril Gonzalez, O. Behnke, A. Belvedere, S. Bhattacharya, F. Blekman[26], K. Borras[27], A. Campbell, A. Cardini, C. Cheng, F. Colombina, S. Consuegra Rodríguez, G. Correia Silva, M. De Silva, G. Eckerlin, D. Eckstein, L.I. Estevez Banos, O. Filatov, E. Gallo[26], A. Geiser, A. Giraldi, V. Guglielmi, M. Guthoff, A. Hinzmann, A. Jafari[28], L. Jeppe, N.Z. Jomhari, B. Kaech, M. Kasemann, C. Kleinwort, R. Kogler, M. Komm, D. Krücker, W. Lange, D. Leyva Pernia, K. Lipka[29], W. Lohmann[30], F. Lorkowski, R. Mankel, I.-A. Melzer-Pellmann, M. Mendizabal Morentin, A.B. Meyer, G. Milella, A. Mussgiller, L.P. Nair, A. Nürnberg, Y. Otarid, J. Park, D. Pérez Adán, E. Ranken, A. Raspereza, D. Rastorguev, B. Ribeiro Lopes, J. Rübenach, A. Saggio, M. Scham[31,27], S. Schnake[27], P. Schütze, C. Schwanenberger[26], D. Selivanova, K. Sharko, M. Shchedrolosiev, R.E. Sosa Ricardo, D. Stafford, F. Vazzoler, A. Ventura Barroso, R. Walsh, Q. Wang, Y. Wen, K. Wichmann, L. Wiens[27], C. Wissing, Y. Yang, A. Zimermmane Castro Santos

University of Hamburg, Hamburg, Germany
A. Albrecht, S. Albrecht, M. Antonello, S. Bein, L. Benato, S. Bollweg, M. Bonanomi, P. Connor, K. El Morabit, Y. Fischer, E. Garutti, A. Grohsjean, J. Haller, H.R. Jabusch, G. Kasieczka, P. Keicher, R. Klanner, W. Korcari, T. Kramer, V. Kutzner, F. Labe, J. Lange, A. Lobanov, C. Matthies, A. Mehta, L. Moureaux, M. Mrowietz, A. Nigamova, Y. Nissan, A. Paasch, K.J. Pena Rodriguez, T. Quadfasel, B. Raciti, M. Rieger, D. Savoiu, J. Schindler, P. Schleper, M. Schröder, J. Schwandt, M. Sommerhalder, H. Stadie, G. Steinbrück, A. Tews, M. Wolf

Karlsruher Institut fuer Technologie, Karlsruhe, Germany
S. Brommer, M. Burkart, E. Butz, T. Chwalek, A. Dierlamm, A. Droll, N. Faltermann, M. Giffels, A. Gottmann, F. Hartmann[32], R. Hofsaess, M. Horzela, U. Husemann, J. Kieseler, M. Klute, R. Koppenhöfer, J.M. Lawhorn, M. Link, A. Lintuluoto, B. Maier, S. Maier, S. Mitra, M. Mormile, Th. Müller, M. Neukum, M. Oh, E. Pfeffer, M. Presilla, G. Quast, K. Rabbertz, B. Regnery, N. Shadskiy, I. Shvetsov, H.J. Simonis, M. Toms, N. Trevisani, R.F. Von Cube, M. Wassmer,

S. Wieland, F. Wittig, R. Wolf, X. Zuo

Institute of Nuclear and Particle Physics (INPP), NCSR Demokritos, Aghia Paraskevi, Greece
G. Anagnostou, G. Daskalakis, A. Kyriakis, A. Papadopoulos[32], A. Stakia

National and Kapodistrian University of Athens, Athens, Greece
P. Kontaxakis, G. Melachroinos, Z. Painesis, A. Panagiotou, I. Papavergou, I. Paraskevas, N. Saoulidou, K. Theofilatos, E. Tziaferi, K. Vellidis, I. Zisopoulos

National Technical University of Athens, Athens, Greece
G. Bakas, T. Chatzistavrou, G. Karapostoli, K. Kousouris, I. Papakrivopoulos, E. Siamarkou, G. Tsipolitis, A. Zacharopoulou

University of Ioánnina, Ioánnina, Greece
K. Adamidis, I. Bestintzanos, I. Evangelou, C. Foudas, C. Kamtsikis, P. Katsoulis, P. Kokkas, P.G. Kosmoglou Kioseoglou, N. Manthos, I. Papadopoulos, J. Strologas

HUN-REN Wigner Research Centre for Physics, Budapest, Hungary
M. Bartók[33], C. Hajdu, D. Horvath[34,35], K. Márton, A.J. Rádl[36], F. Sikler, V. Veszpremi

MTA-ELTE Lendület CMS Particle and Nuclear Physics Group, Eötvös Loránd University, Budapest, Hungary
M. Csanád, K. Farkas, M.M.A. Gadallah[37], Á. Kadlecsik, P. Major, K. Mandal, G. Pásztor, G.I. Veres

Faculty of Informatics, University of Debrecen, Debrecen, Hungary
P. Raics, B. Ujvari, G. Zilizi

Institute of Nuclear Research ATOMKI, Debrecen, Hungary
G. Bencze, S. Czellar, J. Molnar, Z. Szillasi

Karoly Robert Campus, MATE Institute of Technology, Gyongyos, Hungary
T. Csorgo[38], F. Nemes[38], T. Novak

Panjab University, Chandigarh, India
J. Babbar, S. Bansal, S.B. Beri, V. Bhatnagar, G. Chaudhary, S. Chauhan, N. Dhingra[39], A. Kaur, A. Kaur, H. Kaur, M. Kaur, S. Kumar, K. Sandeep, T. Sheokand, J.B. Singh, A. Singla

University of Delhi, Delhi, India
A. Ahmed, A. Bhardwaj, A. Chhetri, B.C. Choudhary, A. Kumar, A. Kumar, M. Naimuddin, K. Ranjan, S. Saumya

Saha Institute of Nuclear Physics, HBNI, Kolkata, India
S. Baradia, S. Barman[40], S. Bhattacharya, S. Dutta, S. Dutta, S. Sarkar

Indian Institute of Technology Madras, Madras, India
M.M. Ameen, P.K. Behera, S.C. Behera, S. Chatterjee, P. Jana, P. Kalbhor, J.R. Komaragiri[41], D. Kumar[41], P.R. Pujahari, N.R. Saha, A. Sharma, A.K. Sikdar, S. Verma

Tata Institute of Fundamental Research-A, Mumbai, India
S. Dugad, M. Kumar, G.B. Mohanty, P. Suryadevara

Tata Institute of Fundamental Research-B, Mumbai, India

A. Bala, S. Banerjee, R.M. Chatterjee, R.K. Dewanjee[42], M. Guchait, Sh. Jain, A. Jaiswal, S. Kumar, G. Majumder, K. Mazumdar, S. Parolia, A. Thachayath

National Institute of Science Education and Research, An OCC of Homi Bhabha National Institute, Bhubaneswar, Odisha, India
S. Bahinipati[43], C. Kar, D. Maity[44], P. Mal, T. Mishra, V.K. Muraleedharan Nair Bindhu[44], K. Naskar[44], A. Nayak[44], P. Sadangi, S.K. Swain, S. Varghese[44], D. Vats[44]

Indian Institute of Science Education and Research (IISER), Pune, India
S. Acharya[45], A. Alpana, S. Dube, B. Gomber[45], B. Kansal, A. Laha, B. Sahu[45], S. Sharma, K.Y. Vaish

Isfahan University of Technology, Isfahan, Iran
H. Bakhshiansohi[46], E. Khazaie[47], M. Zeinali[48]

Institute for Research in Fundamental Sciences (IPM), Tehran, Iran
S. Chenarani[49], S.M. Etesami, M. Khakzad, M. Mohammadi Najafabadi

University College Dublin, Dublin, Ireland
M. Grunewald

INFN Sezione di Bari[a], Università di Bari[b], Politecnico di Bari[c], Bari, Italy
M. Abbrescia[a,b], R. Aly[a,c,50], A. Colaleo[a,b], D. Creanza[a,c], B. D'Anzi[a,b], N. De Filippis[a,c], M. De Palma[a,b], A. Di Florio[a,c], W. Elmetenawee[a,b,50], L. Fiore[a], G. Iaselli[a,c], M. Louka[a,b], G. Maggi[a,c], M. Maggi[a], I. Margjeka[a,b], V. Mastrapasqua[a,b], S. My[a,b], S. Nuzzo[a,b], A. Pellecchia[a,b], A. Pompili[a,b], G. Pugliese[a,c], R. Radogna[a], G. Ramirez-Sanchez[a,c], D. Ramos[a], A. Ranieri[a], L. Silvestris[a], F.M. Simone[a,b], Ü. Sözbilir[a], A. Stamerra[a], R. Venditti[a], P. Verwilligen[a], A. Zaza[a,b]

INFN Sezione di Bologna[a], Università di Bologna[b], Bologna, Italy
G. Abbiendi[a], C. Battilana[a,b], D. Bonacorsi[a,b], L. Borgonovi[a], R. Campanini[a,b], P. Capiluppi[a,b], A. Castro[a,b], F.R. Cavallo[a], M. Cuffiani[a,b], G.M. Dallavalle[a], T. Diotalevi[a,b], F. Fabbri[a], A. Fanfani[a,b], D. Fasanella[a,b], L. Giommi[a,b], C. Grandi[a], L. Guiducci[a,b], S. Lo Meo[a,51], L. Lunerti[a,b], S. Marcellini[a], G. Masetti[a], F.L. Navarria[a,b], A. Perrotta[a], F. Primavera[a,b], A.M. Rossi[a,b], T. Rovelli[a,b], G.P. Siroli[a,b]

INFN Sezione di Catania[a], Università di Catania[b], Catania, Italy
S. Costa[a,b,52], A. Di Mattia[a], R. Potenza[a,b], A. Tricomi[a,b,52], C. Tuve[a,b]

INFN Sezione di Firenze[a], Università di Firenze[b], Firenze, Italy
P. Assiouras[a], G. Barbagli[a], G. Bardelli[a,b], B. Camaiani[a,b], A. Cassese[a], R. Ceccarelli[a], V. Ciulli[a,b], C. Civinini[a], R. D'Alessandro[a,b], E. Focardi[a,b], T. Kello[a], G. Latino[a,b], P. Lenzi[a,b], M. Lizzo[a], M. Meschini[a], S. Paoletti[a], A. Papanastassiou[a,b], G. Sguazzoni[a], L. Viliani[a]

INFN Laboratori Nazionali di Frascati, Frascati, Italy
L. Benussi, S. Bianco, S. Meola[53], D. Piccolo

INFN Sezione di Genova[a], Università di Genova[b], Genova, Italy
P. Chatagnon[a], F. Ferro[a], E. Robutti[a], S. Tosi[a,b]

INFN Sezione di Milano-Bicocca[a], Università di Milano-Bicocca[b], Milano, Italy

A. Benaglia[a], G. Boldrini[a,b], F. Brivio[a], F. Cetorelli[a], F. De Guio[a,b], M.E. Dinardo[a,b], P. Dini[a], S. Gennai[a], R. Gerosa[a,b], A. Ghezzi[a,b], P. Govoni[a,b], L. Guzzi[a], M.T. Lucchini[a,b], M. Malberti[a], S. Malvezzi[a], A. Massironi[a], D. Menasce[a], L. Moroni[a], M. Paganoni[a,b], S. Palluotto[a,b], D. Pedrini[a], B.S. Pinolini[a], G. Pizzati[a,b], S. Ragazzi[a,b], T. Tabarelli de Fatis[a,b], D. Zuolo[a]

INFN Sezione di Napoli[a], Università di Napoli 'Federico II'[b], Napoli, Italy; Università della Basilicata[c], Potenza, Italy; Scuola Superiore Meridionale (SSM)[d], Napoli, Italy
S. Buontempo[a], A. Cagnotta[a,b], F. Carnevali[a,b], N. Cavallo[a,c], F. Fabozzi[a,c], A.O.M. Iorio[a,b], L. Lista[a,b,54], P. Paolucci[a,32], B. Rossi[a], C. Sciacca[a,b]

INFN Sezione di Padova[a], Università di Padova[b], Padova, Italy; Università di Trento[c], Trento, Italy
R. Ardino[a], P. Azzi[a], N. Bacchetta[a,55], D. Bisello[a,b], P. Bortignon[a], G. Bortolato[a,b], A. Bragagnolo[a,b], A.C.M. Bulla[a], P. Checchia[a], T. Dorigo[a], F. Gasparini[a,b], U. Gasparini[a,b], E. Lusiani[a], M. Margoni[a,b], F. Marini[a], A.T. Meneguzzo[a,b], M. Migliorini[a,b], M. Passaseo[a], J. Pazzini[a,b], P. Ronchese[a,b], R. Rossin[a,b], F. Simonetto[a,b], G. Strong[a], M. Tosi[a,b], A. Triossi[a,b], S. Ventura[a], H. Yarar[a,b], M. Zanetti[a,b], P. Zotto[a,b], A. Zucchetta[a,b], G. Zumerle[a,b]

INFN Sezione di Pavia[a], Università di Pavia[b], Pavia, Italy
S. Abu Zeid[a,56], C. Aimè[a,b], A. Braghieri[a], S. Calzaferri[a], D. Fiorina[a], P. Montagna[a,b], V. Re[a], C. Riccardi[a,b], P. Salvini[a], I. Vai[a,b], P. Vitulo[a,b]

INFN Sezione di Perugia[a], Università di Perugia[b], Perugia, Italy
S. Ajmal[a,b], G.M. Bilei[a], D. Ciangottini[a,b], L. Fanò[a,b], M. Magherini[a,b], G. Mantovani[a,b], V. Mariani[a,b], M. Menichelli[a], F. Moscatelli[a,57], A. Rossi[a,b], A. Santocchia[a,b], D. Spiga[a], T. Tedeschi[a,b]

INFN Sezione di Pisa[a], Università di Pisa[b], Scuola Normale Superiore di Pisa[c], Pisa, Italy; Università di Siena[d], Siena, Italy
P. Asenov[a,b], P. Azzurri[a], G. Bagliesi[a], R. Bhattacharya[a], L. Bianchini[a,b], T. Boccali[a], E. Bossini[a], D. Bruschini[a,c], R. Castaldi[a], M.A. Ciocci[a,b], M. Cipriani[a,b], V. D'Amante[a,d], R. Dell'Orso[a], S. Donato[a], A. Giassi[a], F. Ligabue[a,c], D. Matos Figueiredo[a], A. Messineo[a,b], M. Musich[a,b], F. Palla[a], A. Rizzi[a,b], G. Rolandi[a,c], S. Roy Chowdhury[a], T. Sarkar[a], A. Scribano[a], P. Spagnolo[a], R. Tenchini[a], G. Tonelli[a,b], N. Turini[a,d], F. Vaselli[a,c], A. Venturi[a], P.G. Verdini[a]

INFN Sezione di Roma[a], Sapienza Università di Roma[b], Roma, Italy
C. Baldenegro Barrera[a,b], P. Barria[a], C. Basile[a,b], M. Campana[a,b], F. Cavallari[a], L. Cunqueiro Mendez[a,b], D. Del Re[a,b], E. Di Marco[a], M. Diemoz[a], F. Errico[a,b], E. Longo[a,b], P. Meridiani[a], J. Mijuskovic[a,b], G. Organtini[a,b], F. Pandolfi[a], R. Paramatti[a,b], C. Quaranta[a,b], S. Rahatlou[a,b], C. Rovelli[a], F. Santanastasio[a,b], L. Soffi[a]

INFN Sezione di Torino[a], Università di Torino[b], Torino, Italy; Università del Piemonte Orientale[c], Novara, Italy
N. Amapane[a,b], R. Arcidiacono[a,c], S. Argiro[a,b], M. Arneodo[a,c], N. Bartosik[a], R. Bellan[a,b], A. Bellora[a,b], C. Biino[a], C. Borca[a,b], N. Cartiglia[a], M. Costa[a,b], R. Covarelli[a,b], N. Demaria[a], L. Finco[a], M. Grippo[a,b], B. Kiani[a,b], F. Legger[a], F. Luongo[a,b], C. Mariotti[a], L. Markovic[a,b], S. Maselli[a], A. Mecca[a,b], E. Migliore[a,b], M. Monteno[a], R. Mulargia[a], M.M. Obertino[a,b], G. Ortona[a],

L. Pacher[a,b], N. Pastrone[a], M. Pelliccioni[a], M. Ruspa[a,c], F. Siviero[a,b], V. Sola[a,b], A. Solano[a,b], A. Staiano[a], C. Tarricone[a,b], D. Trocino[a], G. Umoret[a,b], E. Vlasov[a,b], R. White[a]

INFN Sezione di Trieste[a], Università di Trieste[b], Trieste, Italy
S. Belforte[a], V. Candelise[a,b], M. Casarsa[a], F. Cossutti[a], K. De Leo[a], G. Della Ricca[a,b]

Kyungpook National University, Daegu, Korea
S. Dogra, J. Hong, C. Huh, B. Kim, D.H. Kim, J. Kim, H. Lee, S.W. Lee, C.S. Moon, Y.D. Oh, M.S. Ryu, S. Sekmen, Y.C. Yang

Department of Mathematics and Physics - GWNU, Gangneung, Korea
M.S. Kim

Chonnam National University, Institute for Universe and Elementary Particles, Kwangju, Korea
G. Bak, P. Gwak, H. Kim, D.H. Moon

Hanyang University, Seoul, Korea
E. Asilar, D. Kim, T.J. Kim, J.A. Merlin

Korea University, Seoul, Korea
S. Choi, S. Han, B. Hong, K. Lee, K.S. Lee, S. Lee, J. Park, S.K. Park, J. Yoo

Kyung Hee University, Department of Physics, Seoul, Korea
J. Goh, S. Yang

Sejong University, Seoul, Korea
H. S. Kim, Y. Kim, S. Lee

Seoul National University, Seoul, Korea
J. Almond, J.H. Bhyun, J. Choi, W. Jun, J. Kim, S. Ko, H. Kwon, H. Lee, J. Lee, J. Lee, B.H. Oh, S.B. Oh, H. Seo, U.K. Yang, I. Yoon

University of Seoul, Seoul, Korea
W. Jang, D.Y. Kang, Y. Kang, S. Kim, B. Ko, J.S.H. Lee, Y. Lee, I.C. Park, Y. Roh, I.J. Watson

Yonsei University, Department of Physics, Seoul, Korea
S. Ha, H.D. Yoo

Sungkyunkwan University, Suwon, Korea
M. Choi, M.R. Kim, H. Lee, Y. Lee, I. Yu

College of Engineering and Technology, American University of the Middle East (AUM), Dasman, Kuwait
T. Beyrouthy

Riga Technical University, Riga, Latvia
K. Dreimanis, A. Gaile, G. Pikurs, A. Potrebko, M. Seidel

University of Latvia (LU), Riga, Latvia
N.R. Strautnieks

Vilnius University, Vilnius, Lithuania
M. Ambrozas, A. Juodagalvis, A. Rinkevicius, G. Tamulaitis

National Centre for Particle Physics, Universiti Malaya, Kuala Lumpur, Malaysia
N. Bin Norjoharuddeen, I. Yusuff[58], Z. Zolkapli

Universidad de Sonora (UNISON), Hermosillo, Mexico
J.F. Benitez, A. Castaneda Hernandez, H.A. Encinas Acosta, L.G. Gallegos Maríñez, M. León Coello, J.A. Murillo Quijada, A. Sehrawat, L. Valencia Palomo

Centro de Investigacion y de Estudios Avanzados del IPN, Mexico City, Mexico
G. Ayala, H. Castilla-Valdez, H. Crotte Ledesma, E. De La Cruz-Burelo, I. Heredia-De La Cruz[59], R. Lopez-Fernandez, C.A. Mondragon Herrera, A. Sánchez Hernández

Universidad Iberoamericana, Mexico City, Mexico
C. Oropeza Barrera, M. Ramírez García

Benemerita Universidad Autonoma de Puebla, Puebla, Mexico
I. Bautista, I. Pedraza, H.A. Salazar Ibarguen, C. Uribe Estrada

University of Montenegro, Podgorica, Montenegro
I. Bubanja, N. Raicevic

University of Canterbury, Christchurch, New Zealand
P.H. Butler

National Centre for Physics, Quaid-I-Azam University, Islamabad, Pakistan
A. Ahmad, M.I. Asghar, A. Awais, M.I.M. Awan, H.R. Hoorani, W.A. Khan

AGH University of Krakow, Faculty of Computer Science, Electronics and Telecommunications, Krakow, Poland
V. Avati, L. Grzanka, M. Malawski

National Centre for Nuclear Research, Swierk, Poland
H. Bialkowska, M. Bluj, B. Boimska, M. Górski, M. Kazana, M. Szleper, P. Zalewski

Institute of Experimental Physics, Faculty of Physics, University of Warsaw, Warsaw, Poland
K. Bunkowski, K. Doroba, A. Kalinowski, M. Konecki, J. Krolikowski, A. Muhammad

Warsaw University of Technology, Warsaw, Poland
K. Pozniak, W. Zabolotny

Laboratório de Instrumentação e Física Experimental de Partículas, Lisboa, Portugal
M. Araujo, D. Bastos, C. Beirão Da Cruz E Silva, A. Boletti, M. Bozzo, T. Camporesi, G. Da Molin, P. Faccioli, M. Gallinaro, J. Hollar, N. Leonardo, T. Niknejad, A. Petrilli, M. Pisano, J. Seixas, J. Varela, J.W. Wulff

Faculty of Physics, University of Belgrade, Belgrade, Serbia
P. Adzic, P. Milenovic

VINCA Institute of Nuclear Sciences, University of Belgrade, Belgrade, Serbia
M. Dordevic, J. Milosevic, V. Rekovic

Centro de Investigaciones Energéticas Medioambientales y Tecnológicas (CIEMAT), Madrid, Spain
M. Aguilar-Benitez, J. Alcaraz Maestre, Cristina F. Bedoya, Oliver M. Carretero, M. Cepeda, M. Cerrada, N. Colino, B. De La Cruz, A. Delgado Peris, A. Escalante Del Valle, D. Fernández Del Val, J.P. Fernández Ramos, J. Flix,

M.C. Fouz, O. Gonzalez Lopez, S. Goy Lopez, J.M. Hernandez, M.I. Josa, D. Moran, C. M. Morcillo Perez, Á. Navarro Tobar, C. Perez Dengra, A. Pérez-Calero Yzquierdo, J. Puerta Pelayo, I. Redondo, D.D. Redondo Ferrero, L. Romero, S. Sánchez Navas, L. Urda Gómez, J. Vazquez Escobar, C. Willmott

Universidad Autónoma de Madrid, Madrid, Spain
J.F. de Trocóniz

Universidad de Oviedo, Instituto Universitario de Ciencias y Tecnologías Espaciales de Asturias (ICTEA), Oviedo, Spain
B. Alvarez Gonzalez, J. Cuevas, J. Fernandez Menendez, S. Folgueras, I. Gonzalez Caballero, J.R. González Fernández, P. Leguina, E. Palencia Cortezon, C. Ramón Álvarez, V. Rodríguez Bouza, A. Soto Rodríguez, A. Trapote, C. Vico Villalba, P. Vischia

Instituto de Física de Cantabria (IFCA), CSIC-Universidad de Cantabria, Santander, Spain
S. Bhowmik, S. Blanco Fernández, J.A. Brochero Cifuentes, I.J. Cabrillo, A. Calderon, J. Duarte Campderros, M. Fernandez, G. Gomez, C. Lasaosa García, R. Lopez Ruiz, C. Martinez Rivero, P. Martinez Ruiz del Arbol, F. Matorras, P. Matorras Cuevas, E. Navarrete Ramos, J. Piedra Gomez, L. Scodellaro, I. Vila, J.M. Vizan Garcia

University of Colombo, Colombo, Sri Lanka
M.K. Jayananda, B. Kailasapathy[60], D.U.J. Sonnadara, D.D.C. Wickramarathna

University of Ruhuna, Department of Physics, Matara, Sri Lanka
W.G.D. Dharmaratna[61], K. Liyanage, N. Perera, N. Wickramage

CERN, European Organization for Nuclear Research, Geneva, Switzerland
D. Abbaneo, C. Amendola, E. Auffray, G. Auzinger, J. Baechler, D. Barney, A. Bermúdez Martínez, M. Bianco, B. Bilin, A.A. Bin Anuar, A. Bocci, C. Botta, E. Brondolin, C. Caillol, G. Cerminara, N. Chernyavskaya, D. d'Enterria, A. Dabrowski, A. David, A. De Roeck, M.M. Defranchis, M. Deile, M. Dobson, L. Forthomme, G. Franzoni, W. Funk, S. Giani, D. Gigi, K. Gill, F. Glege, L. Gouskos, M. Haranko, J. Hegeman, B. Huber, V. Innocente, T. James, P. Janot, O. Kaluzinska, S. Laurila, P. Lecoq, E. Leutgeb, C. Lourenço, L. Malgeri, M. Mannelli, A.C. Marini, M. Matthewman, F. Meijers, S. Mersi, E. Meschi, V. Milosevic, F. Monti, F. Moortgat, M. Mulders, I. Neutelings, S. Orfanelli, F. Pantaleo, G. Petrucciani, A. Pfeiffer, M. Pierini, D. Piparo, H. Qu, D. Rabady, M. Rovere, H. Sakulin, S. Scarfi, C. Schwick, M. Selvaggi, A. Sharma, K. Shchelina, P. Silva, P. Sphicas[62], A.G. Stahl Leiton, A. Steen, S. Summers, D. Treille, P. Tropea, A. Tsirou, D. Walter, J. Wanczyk[63], J. Wang, S. Wuchterl, P. Zehetner, P. Zejdl, W.D. Zeuner

Paul Scherrer Institut, Villigen, Switzerland
T. Bevilacqua[64], L. Caminada[64], A. Ebrahimi, W. Erdmann, R. Horisberger, Q. Ingram, H.C. Kaestli, D. Kotlinski, C. Lange, M. Missiroli[64], L. Noehte[64], T. Rohe

ETH Zurich - Institute for Particle Physics and Astrophysics (IPA), Zurich, Switzerland
T.K. Aarrestad, K. Androsov[63], M. Backhaus, G. Bonomelli, A. Calandri, C. Cazzaniga, K. Datta, A. De Cosa, G. Dissertori, M. Dittmar, M. Donegà, F. Eble, M. Galli, K. Gedia, F. Glessgen, C. Grab, N. Härringer, T.G. Harte, D. Hits,

W. Lustermann, A.-M. Lyon, R.A. Manzoni, M. Marchegiani, L. Marchese, C. Martin Perez, A. Mascellani[63], F. Nessi-Tedaldi, F. Pauss, V. Perovic, S. Pigazzini, C. Reissel, T. Reitenspiess, B. Ristic, F. Riti, R. Seidita, J. Steggemann[63], D. Valsecchi, R. Wallny

Universität Zürich, Zurich, Switzerland
C. Amsler[65], P. Bärtschi, M.F. Canelli, K. Cormier, J.K. Heikkilä, M. Huwiler, W. Jin, A. Jofrehei, B. Kilminster, S. Leontsinis, S.P. Liechti, A. Macchiolo, P. Meiring, U. Molinatti, A. Reimers, P. Robmann, S. Sanchez Cruz, M. Senger, F. Stäger, Y. Takahashi, R. Tramontano

National Central University, Chung-Li, Taiwan
C. Adloff[66], D. Bhowmik, C.M. Kuo, W. Lin, P.K. Rout, P.C. Tiwari[41], S.S. Yu

National Taiwan University (NTU), Taipei, Taiwan
L. Ceard, Y. Chao, K.F. Chen, P.s. Chen, Z.g. Chen, A. De Iorio, W.-S. Hou, T.h. Hsu, Y.w. Kao, S. Karmakar, R. Khurana, G. Kole, Y.y. Li, R.-S. Lu, E. Paganis, X.f. Su, J. Thomas-Wilsker, L.s. Tsai, H.y. Wu, E. Yazgan

High Energy Physics Research Unit, Department of Physics, Faculty of Science, Chulalongkorn University, Bangkok, Thailand
C. Asawatangtrakuldee, N. Srimanobhas, V. Wachirapusitanand

Çukurova University, Physics Department, Science and Art Faculty, Adana, Turkey
D. Agyel, F. Boran, Z.S. Demiroglu, F. Dolek, I. Dumanoglu[67], E. Eskut, Y. Guler[68], E. Gurpinar Guler[68], C. Isik, O. Kara, A. Kayis Topaksu, U. Kiminsu, G. Onengut, K. Ozdemir[69], A. Polatoz, B. Tali[70], U.G. Tok, S. Turkcapar, E. Uslan, I.S. Zorbakir

Middle East Technical University, Physics Department, Ankara, Turkey
G. Sokmen, M. Yalvac[71]

Bogazici University, Istanbul, Turkey
B. Akgun, I.O. Atakisi, E. Gülmez, M. Kaya[72], O. Kaya[73], S. Tekten[74]

Istanbul Technical University, Istanbul, Turkey
A. Cakir, K. Cankocak[67,75], G.G. Dincer, Y. Komurcu, S. Sen[76]

Istanbul University, Istanbul, Turkey
O. Aydilek[25], S. Cerci[70], V. Epshteyn, B. Hacisahinoglu, I. Hos[77], B. Kaynak, S. Ozkorucuklu, O. Potok, H. Sert, C. Simsek, C. Zorbilmez

Yildiz Technical University, Istanbul, Turkey
B. Isildak[78], D. Sunar Cerci[70]

Institute for Scintillation Materials of National Academy of Science of Ukraine, Kharkiv, Ukraine
A. Boyaryntsev, B. Grynyov

National Science Centre, Kharkiv Institute of Physics and Technology, Kharkiv, Ukraine
L. Levchuk

University of Bristol, Bristol, United Kingdom
D. Anthony, J.J. Brooke, A. Bundock, F. Bury, E. Clement, D. Cussans, H. Flacher, M. Glowacki, J. Goldstein, H.F. Heath, M.-L. Holmberg, L. Kreczko, S. Paramesvaran, L. Robertshaw, S. Seif El Nasr-Storey, V.J. Smith, N. Stylianou[79],

K. Walkingshaw Pass

Rutherford Appleton Laboratory, Didcot, United Kingdom
A.H. Ball, K.W. Bell, A. Belyaev[80], C. Brew, R.M. Brown, D.J.A. Cockerill, C. Cooke, K.V. Ellis, K. Harder, S. Harper, J. Linacre, K. Manolopoulos, D.M. Newbold, E. Olaiya, D. Petyt, T. Reis, A.R. Sahasransu, G. Salvi, T. Schuh, C.H. Shepherd-Themistocleous, I.R. Tomalin, T. Williams

Imperial College, London, United Kingdom
R. Bainbridge, P. Bloch, C.E. Brown, O. Buchmuller, V. Cacchio, C.A. Carrillo Montoya, G.S. Chahal[81], D. Colling, J.S. Dancu, I. Das, P. Dauncey, G. Davies, J. Davies, M. Della Negra, S. Fayer, G. Fedi, G. Hall, M.H. Hassanshahi, A. Howard, G. Iles, M. Knight, J. Langford, J. León Holgado, L. Lyons, A.-M. Magnan, S. Malik, M. Mieskolainen, J. Nash[82], M. Pesaresi, B.C. Radburn-Smith, A. Richards, A. Rose, K. Savva, C. Seez, R. Shukla, A. Tapper, K. Uchida, G.P. Uttley, L.H. Vage, T. Virdee[32], M. Vojinovic, N. Wardle, D. Winterbottom

Brunel University, Uxbridge, United Kingdom
K. Coldham, J.E. Cole, A. Khan, P. Kyberd, I.D. Reid

Baylor University, Waco, Texas, USA
S. Abdullin, A. Brinkerhoff, B. Caraway, E. Collins, J. Dittmann, K. Hatakeyama, J. Hiltbrand, B. McMaster, M. Saunders, S. Sawant, C. Sutantawibul, J. Wilson

Catholic University of America, Washington, DC, USA
R. Bartek, A. Dominguez, C. Huerta Escamilla, A.E. Simsek, R. Uniyal, A.M. Vargas Hernandez

The University of Alabama, Tuscaloosa, Alabama, USA
B. Bam, R. Chudasama, S.I. Cooper, S.V. Gleyzer, C.U. Perez, P. Rumerio[83], E. Usai, R. Yi

Boston University, Boston, Massachusetts, USA
A. Akpinar, D. Arcaro, C. Cosby, Z. Demiragli, C. Erice, C. Fangmeier, C. Fernandez Madrazo, E. Fontanesi, D. Gastler, F. Golf, S. Jeon, I. Reed, J. Rohlf, K. Salyer, D. Sperka, D. Spitzbart, I. Suarez, A. Tsatsos, S. Yuan, A.G. Zecchinelli

Brown University, Providence, Rhode Island, USA
G. Benelli, X. Coubez[27], D. Cutts, M. Hadley, U. Heintz, J.M. Hogan[84], T. Kwon, G. Landsberg, K.T. Lau, D. Li, J. Luo, S. Mondal, M. Narain[†], N. Pervan, S. Sagir[85], F. Simpson, M. Stamenkovic, X. Yan, W. Zhang

University of California, Davis, Davis, California, USA
S. Abbott, J. Bonilla, C. Brainerd, R. Breedon, H. Cai, M. Calderon De La Barca Sanchez, M. Chertok, M. Citron, J. Conway, P.T. Cox, R. Erbacher, F. Jensen, O. Kukral, G. Mocellin, M. Mulhearn, D. Pellett, W. Wei, Y. Yao, F. Zhang

University of California, Los Angeles, California, USA
M. Bachtis, R. Cousins, A. Datta, G. Flores Avila, J. Hauser, M. Ignatenko, M.A. Iqbal, T. Lam, E. Manca, A. Nunez Del Prado, D. Saltzberg, V. Valuev

University of California, Riverside, Riverside, California, USA
R. Clare, J.W. Gary, M. Gordon, G. Hanson, W. Si, S. Wimpenny[†]

University of California, San Diego, La Jolla, California, USA
J.G. Branson, S. Cittolin, S. Cooperstein, D. Diaz, J. Duarte, L. Giannini, J. Guiang, R. Kansal, V. Krutelyov, R. Lee, J. Letts, M. Masciovecchio, F. Mokhtar, S. Mukherjee, M. Pieri, M. Quinnan, B.V. Sathia Narayanan, V. Sharma, M. Tadel, E. Vourliotis, F. Würthwein, Y. Xiang, A. Yagil

University of California, Santa Barbara - Department of Physics, Santa Barbara, California, USA
A. Barzdukas, L. Brennan, C. Campagnari, J. Incandela, J. Kim, A.J. Li, P. Masterson, H. Mei, J. Richman, U. Sarica, R. Schmitz, F. Setti, J. Sheplock, D. Stuart, T.Á. Vámi, S. Wang

California Institute of Technology, Pasadena, California, USA
A. Bornheim, O. Cerri, A. Latorre, J. Mao, H.B. Newman, G. Reales Gutiérrez, M. Spiropulu, J.R. Vlimant, C. Wang, S. Xie, R.Y. Zhu

Carnegie Mellon University, Pittsburgh, Pennsylvania, USA
J. Alison, S. An, M.B. Andrews, P. Bryant, M. Cremonesi, V. Dutta, T. Ferguson, A. Harilal, C. Liu, T. Mudholkar, S. Murthy, P. Palit, M. Paulini, A. Roberts, A. Sanchez, W. Terrill

University of Colorado Boulder, Boulder, Colorado, USA
J.P. Cumalat, W.T. Ford, A. Hart, A. Hassani, G. Karathanasis, N. Manganelli, A. Perloff, C. Savard, N. Schonbeck, K. Stenson, K.A. Ulmer, S.R. Wagner, N. Zipper

Cornell University, Ithaca, New York, USA
J. Alexander, S. Bright-Thonney, X. Chen, D.J. Cranshaw, J. Fan, X. Fan, S. Hogan, P. Kotamnives, J. Monroy, M. Oshiro, J.R. Patterson, J. Reichert, M. Reid, A. Ryd, J. Thom, P. Wittich, R. Zou

Fermi National Accelerator Laboratory, Batavia, Illinois, USA
M. Albrow, M. Alyari, O. Amram, G. Apollinari, A. Apresyan, L.A.T. Bauerdick, D. Berry, J. Berryhill, P.C. Bhat, K. Burkett, J.N. Butler, A. Canepa, G.B. Cerati, H.W.K. Cheung, F. Chlebana, G. Cummings, J. Dickinson, I. Dutta, V.D. Elvira, Y. Feng, J. Freeman, A. Gandrakota, Z. Gecse, L. Gray, D. Green, A. Grummer, S. Grünendahl, D. Guerrero, O. Gutsche, R.M. Harris, R. Heller, T.C. Herwig, J. Hirschauer, L. Horyn, B. Jayatilaka, S. Jindariani, M. Johnson, U. Joshi, T. Klijnsma, B. Klima, K.H.M. Kwok, S. Lammel, D. Lincoln, R. Lipton, T. Liu, C. Madrid, K. Maeshima, C. Mantilla, D. Mason, P. McBride, P. Merkel, S. Mrenna, S. Nahn, J. Ngadiuba, D. Noonan, V. Papadimitriou, N. Pastika, K. Pedro, C. Pena[86], F. Ravera, A. Reinsvold Hall[87], L. Ristori, E. Sexton-Kennedy, N. Smith, A. Soha, L. Spiegel, S. Stoynev, J. Strait, L. Taylor, S. Tkaczyk, N.V. Tran, L. Uplegger, E.W. Vaandering, A. Whitbeck, I. Zoi

University of Florida, Gainesville, Florida, USA
C. Aruta, P. Avery, D. Bourilkov, L. Cadamuro, P. Chang, V. Cherepanov, R.D. Field, E. Koenig, M. Kolosova, J. Konigsberg, A. Korytov, K. Matchev, N. Menendez, G. Mitselmakher, K. Mohrman, A. Muthirakalayil Madhu, N. Rawal, D. Rosenzweig, S. Rosenzweig, J. Wang

Florida State University, Tallahassee, Florida, USA
T. Adams, A. Al Kadhim, A. Askew, S. Bower, R. Habibullah, V. Hagopian,

R. Hashmi, R.S. Kim, S. Kim, T. Kolberg, G. Martinez, H. Prosper, P.R. Prova, M. Wulansatiti, R. Yohay, J. Zhang

Florida Institute of Technology, Melbourne, Florida, USA
B. Alsufyani, M.M. Baarmand, S. Butalla, S. Das, T. Elkafrawy[56], M. Hohlmann, R. Kumar Verma, M. Rahmani, E. Yanes

University of Illinois Chicago, Chicago, USA, Chicago, USA
M.R. Adams, A. Baty, C. Bennett, R. Cavanaugh, R. Escobar Franco, O. Evdokimov, C.E. Gerber, M. Hawksworth, A. Hingrajiya, D.J. Hofman, J.h. Lee, D. S. Lemos, A.H. Merrit, C. Mills, S. Nanda, G. Oh, B. Ozek, D. Pilipovic, R. Pradhan, E. Prifti, T. Roy, S. Rudrabhatla, M.B. Tonjes, N. Varelas, Z. Ye, J. Yoo

The University of Iowa, Iowa City, Iowa, USA
M. Alhusseini, D. Blend, K. Dilsiz[88], L. Emediato, G. Karaman, O.K. Köseyan, J.-P. Merlo, A. Mestvirishvili[89], J. Nachtman, O. Neogi, H. Ogul[90], Y. Onel, A. Penzo, C. Snyder, E. Tiras[91]

Johns Hopkins University, Baltimore, Maryland, USA
B. Blumenfeld, L. Corcodilos, J. Davis, A.V. Gritsan, L. Kang, S. Kyriacou, P. Maksimovic, M. Roguljic, J. Roskes, S. Sekhar, M. Swartz

The University of Kansas, Lawrence, Kansas, USA
A. Abreu, L.F. Alcerro Alcerro, J. Anguiano, P. Baringer, A. Bean, Z. Flowers, D. Grove, J. King, G. Krintiras, M. Lazarovits, C. Le Mahieu, J. Marquez, N. Minafra, M. Murray, M. Nickel, M. Pitt, S. Popescu[92], C. Rogan, C. Royon, R. Salvatico, S. Sanders, C. Smith, Q. Wang, G. Wilson

Kansas State University, Manhattan, Kansas, USA
B. Allmond, A. Ivanov, K. Kaadze, A. Kalogeropoulos, D. Kim, Y. Maravin, J. Natoli, D. Roy, G. Sorrentino

Lawrence Livermore National Laboratory, Livermore, California, USA
F. Rebassoo, D. Wright

University of Maryland, College Park, Maryland, USA
A. Baden, A. Belloni, Y.M. Chen, S.C. Eno, N.J. Hadley, S. Jabeen, R.G. Kellogg, T. Koeth, Y. Lai, S. Lascio, A.C. Mignerey, S. Nabili, C. Palmer, C. Papageorgakis, M.M. Paranjpe, L. Wang

Massachusetts Institute of Technology, Cambridge, Massachusetts, USA
J. Bendavid, I.A. Cali, M. D'Alfonso, J. Eysermans, C. Freer, G. Gomez-Ceballos, M. Goncharov, G. Grosso, P. Harris, D. Hoang, D. Kovalskyi, J. Krupa, L. Lavezzo, Y.-J. Lee, K. Long, A. Novak, C. Paus, D. Rankin, C. Roland, G. Roland, S. Rothman, G.S.F. Stephans, Z. Wang, B. Wyslouch, T. J. Yang

University of Minnesota, Minneapolis, Minnesota, USA
B. Crossman, B.M. Joshi, C. Kapsiak, M. Krohn, D. Mahon, J. Mans, B. Marzocchi, S. Pandey, M. Revering, R. Rusack, R. Saradhy, N. Schroeder, N. Strobbe, M.A. Wadud

University of Mississippi, Oxford, Mississippi, USA
L.M. Cremaldi

University of Nebraska-Lincoln, Lincoln, Nebraska, USA
K. Bloom, D.R. Claes, G. Haza, J. Hossain, C. Joo, I. Kravchenko, J.E. Siado, W. Tabb, A. Vagnerini, A. Wightman, F. Yan, D. Yu

State University of New York at Buffalo, Buffalo, New York, USA
H. Bandyopadhyay, L. Hay, I. Iashvili, A. Kharchilava, M. Morris, D. Nguyen, S. Rappoccio, H. Rejeb Sfar, A. Williams

Northeastern University, Boston, Massachusetts, USA
G. Alverson, E. Barberis, J. Dervan, Y. Haddad, Y. Han, A. Krishna, J. Li, M. Lu, G. Madigan, R. Mccarthy, D.M. Morse, V. Nguyen, T. Orimoto, A. Parker, L. Skinnari, B. Wang, D. Wood

Northwestern University, Evanston, Illinois, USA
S. Bhattacharya, J. Bueghly, Z. Chen, S. Dittmer, K.A. Hahn, Y. Liu, Y. Miao, D.G. Monk, M.H. Schmitt, A. Taliercio, M. Velasco

University of Notre Dame, Notre Dame, Indiana, USA
G. Agarwal, R. Band, R. Bucci, S. Castells, A. Das, R. Goldouzian, M. Hildreth, K.W. Ho, K. Hurtado Anampa, T. Ivanov, C. Jessop, K. Lannon, J. Lawrence, N. Loukas, L. Lutton, J. Mariano, N. Marinelli, I. Mcalister, T. McCauley, C. Mcgrady, C. Moore, Y. Musienko[16], H. Nelson, M. Osherson, A. Piccinelli, R. Ruchti, A. Townsend, Y. Wan, M. Wayne, H. Yockey, M. Zarucki, L. Zygala

The Ohio State University, Columbus, Ohio, USA
A. Basnet, B. Bylsma, M. Carrigan, L.S. Durkin, C. Hill, M. Joyce, M. Nunez Ornelas, K. Wei, B.L. Winer, B. R. Yates

Princeton University, Princeton, New Jersey, USA
F.M. Addesa, H. Bouchamaoui, P. Das, G. Dezoort, P. Elmer, A. Frankenthal, B. Greenberg, N. Haubrich, G. Kopp, S. Kwan, D. Lange, A. Loeliger, D. Marlow, I. Ojalvo, J. Olsen, A. Shevelev, D. Stickland, C. Tully

University of Puerto Rico, Mayaguez, Puerto Rico, USA
S. Malik

Purdue University, West Lafayette, Indiana, USA
A.S. Bakshi, V.E. Barnes, S. Chandra, R. Chawla, A. Gu, L. Gutay, M. Jones, A.W. Jung, D. Kondratyev, A.M. Koshy, M. Liu, G. Negro, N. Neumeister, G. Paspalaki, S. Piperov, V. Scheurer, J.F. Schulte, M. Stojanovic, J. Thieman, A. K. Virdi, F. Wang, W. Xie

Purdue University Northwest, Hammond, Indiana, USA
J. Dolen, N. Parashar, A. Pathak

Rice University, Houston, Texas, USA
D. Acosta, T. Carnahan, K.M. Ecklund, P.J. Fernández Manteca, S. Freed, P. Gardner, F.J.M. Geurts, W. Li, O. Miguel Colin, B.P. Padley, R. Redjimi, J. Rotter, E. Yigitbasi, Y. Zhang

University of Rochester, Rochester, New York, USA
A. Bodek, P. de Barbaro, R. Demina, J.L. Dulemba, A. Garcia-Bellido, O. Hindrichs, A. Khukhunaishvili, N. Parmar, P. Parygin[93], E. Popova[93], R. Taus

The Rockefeller University, New York, New York, USA

K. Goulianos

Rutgers, The State University of New Jersey, Piscataway, New Jersey, USA
B. Chiarito, J.P. Chou, S.V. Clark, D. Gadkari, Y. Gershtein, E. Halkiadakis, M. Heindl, C. Houghton, D. Jaroslawski, O. Karacheban[30], I. Laflotte, A. Lath, R. Montalvo, K. Nash, H. Routray, P. Saha, S. Salur, S. Schnetzer, S. Somalwar, R. Stone, S.A. Thayil, S. Thomas, J. Vora, H. Wang

University of Tennessee, Knoxville, Tennessee, USA
H. Acharya, D. Ally, A.G. Delannoy, S. Fiorendi, S. Higginbotham, T. Holmes, A.R. Kanuganti, N. Karunarathna, L. Lee, E. Nibigira, S. Spanier

Texas A&M University, College Station, Texas, USA
D. Aebi, M. Ahmad, O. Bouhali[94], R. Eusebi, J. Gilmore, T. Huang, T. Kamon[95], H. Kim, S. Luo, R. Mueller, D. Overton, D. Rathjens, A. Safonov

Texas Tech University, Lubbock, Texas, USA
N. Akchurin, J. Damgov, V. Hegde, A. Hussain, Y. Kazhykarim, K. Lamichhane, S.W. Lee, A. Mankel, T. Peltola, I. Volobouev

Vanderbilt University, Nashville, Tennessee, USA
E. Appelt, Y. Chen, S. Greene, A. Gurrola, W. Johns, R. Kunnawalkam Elayavalli, A. Melo, F. Romeo, P. Sheldon, S. Tuo, J. Velkovska, J. Viinikainen

University of Virginia, Charlottesville, Virginia, USA
B. Cardwell, B. Cox, J. Hakala, R. Hirosky, A. Ledovskoy, C. Neu, C.E. Perez Lara

Wayne State University, Detroit, Michigan, USA
P.E. Karchin

University of Wisconsin - Madison, Madison, Wisconsin, USA
A. Aravind, S. Banerjee, K. Black, T. Bose, S. Dasu, I. De Bruyn, P. Everaerts, C. Galloni, H. He, M. Herndon, A. Herve, C.K. Koraka, A. Lanaro, R. Loveless, J. Madhusudanan Sreekala, A. Mallampalli, A. Mohammadi, S. Mondal, G. Parida, L. Pétré, D. Pinna, A. Savin, V. Shang, V. Sharma, W.H. Smith, D. Teague, H.F. Tsoi, W. Vetens, A. Warden

Authors affiliated with an institute or an international laboratory covered by a cooperation agreement with CERN
S. Afanasiev, V. Andreev, Yu. Andreev, T. Aushev, M. Azarkin, I. Azhgirey, A. Babaev, A. Belyaev, V. Blinov[96], E. Boos, V. Borshch, D. Budkouski, V. Bunichev, V. Chekhovsky, R. Chistov[96], M. Danilov[96], A. Dermenev, T. Dimova[96], D. Druzhkin[97], M. Dubinin[86], L. Dudko, A. Ershov, G. Gavrilov, V. Gavrilov, S. Gninenko, V. Golovtcov, N. Golubev, I. Golutvin, I. Gorbunov, A. Gribushin, Y. Ivanov, V. Kachanov, V. Karjavine, A. Karneyeu, V. Kim[96], M. Kirakosyan, D. Kirpichnikov, M. Kirsanov, V. Klyukhin, O. Kodolova[98], D. Konstantinov, V. Korenkov, A. Kozyrev[96], N. Krasnikov, A. Lanev, P. Levchenko[99], N. Lychkovskaya, V. Makarenko, A. Malakhov, V. Matveev[96], V. Murzin, A. Nikitenko[100,98], S. Obraztsov, V. Oreshkin, V. Palichik, V. Perelygin, M. Perfilov, S. Petrushanko, S. Polikarpov[96], V. Popov, O. Radchenko[96], R. Ryutin, M. Savina, V. Savrin, V. Shalaev, S. Shmatov, S. Shulha, Y. Skovpen[96], S. Slabospitskii, V. Smirnov, D. Sosnov, V. Sulimov, E. Tcherniaev, A. Terkulov, O. Teryaev, I. Tlisova, A. Toropin, L. Uvarov, A. Uzunian, A. Vorobyev[†], N. Voytishin,

B.S. Yuldashev[101], A. Zarubin, I. Zhizhin, A. Zhokin

†: Deceased
[1]Also at Yerevan State University, Yerevan, Armenia
[2]Also at TU Wien, Vienna, Austria
[3]Also at Institute of Basic and Applied Sciences, Faculty of Engineering, Arab Academy for Science, Technology and Maritime Transport, Alexandria, Egypt
[4]Also at Ghent University, Ghent, Belgium
[5]Also at Universidade Estadual de Campinas, Campinas, Brazil
[6]Also at Federal University of Rio Grande do Sul, Porto Alegre, Brazil
[7]Also at UFMS, Nova Andradina, Brazil
[8]Also at Nanjing Normal University, Nanjing, China
[9]Now at The University of Iowa, Iowa City, Iowa, USA
[10]Also at University of Chinese Academy of Sciences, Beijing, China
[11]Also at China Center of Advanced Science and Technology, Beijing, China
[12]Also at University of Chinese Academy of Sciences, Beijing, China
[13]Also at China Spallation Neutron Source, Guangdong, China
[14]Now at Henan Normal University, Xinxiang, China
[15]Also at Université Libre de Bruxelles, Bruxelles, Belgium
[16]Also at an institute or an international laboratory covered by a cooperation agreement with CERN
[17]Also at Cairo University, Cairo, Egypt
[18]Also at Suez University, Suez, Egypt
[19]Now at British University in Egypt, Cairo, Egypt
[20]Also at Purdue University, West Lafayette, Indiana, USA
[21]Also at Université de Haute Alsace, Mulhouse, France
[22]Also at Department of Physics, Tsinghua University, Beijing, China
[23]Also at Tbilisi State University, Tbilisi, Georgia
[24]Also at The University of the State of Amazonas, Manaus, Brazil
[25]Also at Erzincan Binali Yildirim University, Erzincan, Turkey
[26]Also at University of Hamburg, Hamburg, Germany
[27]Also at RWTH Aachen University, III. Physikalisches Institut A, Aachen, Germany
[28]Also at Isfahan University of Technology, Isfahan, Iran
[29]Also at Bergische University Wuppertal (BUW), Wuppertal, Germany
[30]Also at Brandenburg University of Technology, Cottbus, Germany
[31]Also at Forschungszentrum Jülich, Juelich, Germany
[32]Also at CERN, European Organization for Nuclear Research, Geneva, Switzerland
[33]Also at Institute of Physics, University of Debrecen, Debrecen, Hungary
[34]Also at Institute of Nuclear Research ATOMKI, Debrecen, Hungary
[35]Now at Universitatea Babes-Bolyai - Facultatea de Fizica, Cluj-Napoca, Romania
[36]Also at MTA-ELTE Lendület CMS Particle and Nuclear Physics Group, Eötvös Loránd University, Budapest, Hungary
[37]Also at Physics Department, Faculty of Science, Assiut University, Assiut, Egypt
[38]Also at HUN-REN Wigner Research Centre for Physics, Budapest, Hungary
[39]Also at Punjab Agricultural University, Ludhiana, India
[40]Also at University of Visva-Bharati, Santiniketan, India
[41]Also at Indian Institute of Science (IISc), Bangalore, India
[42]Also at Birla Institute of Technology, Mesra, Mesra, India
[43]Also at IIT Bhubaneswar, Bhubaneswar, India
[44]Also at Institute of Physics, Bhubaneswar, India

[45]Also at University of Hyderabad, Hyderabad, India
[46]Also at Deutsches Elektronen-Synchrotron, Hamburg, Germany
[47]Also at Department of Physics, Isfahan University of Technology, Isfahan, Iran
[48]Also at Sharif University of Technology, Tehran, Iran
[49]Also at Department of Physics, University of Science and Technology of Mazandaran, Behshahr, Iran
[50]Also at Helwan University, Cairo, Egypt
[51]Also at Italian National Agency for New Technologies, Energy and Sustainable Economic Development, Bologna, Italy
[52]Also at Centro Siciliano di Fisica Nucleare e di Struttura Della Materia, Catania, Italy
[53]Also at Università degli Studi Guglielmo Marconi, Roma, Italy
[54]Also at Scuola Superiore Meridionale, Università di Napoli 'Federico II', Napoli, Italy
[55]Also at Fermi National Accelerator Laboratory, Batavia, Illinois, USA
[56]Also at Ain Shams University, Cairo, Egypt
[57]Also at Consiglio Nazionale delle Ricerche - Istituto Officina dei Materiali, Perugia, Italy
[58]Also at Department of Applied Physics, Faculty of Science and Technology, Universiti Kebangsaan Malaysia, Bangi, Malaysia
[59]Also at Consejo Nacional de Ciencia y Tecnología, Mexico City, Mexico
[60]Also at Trincomalee Campus, Eastern University, Sri Lanka, Nilaveli, Sri Lanka
[61]Also at Saegis Campus, Nugegoda, Sri Lanka
[62]Also at National and Kapodistrian University of Athens, Athens, Greece
[63]Also at Ecole Polytechnique Fédérale Lausanne, Lausanne, Switzerland
[64]Also at Universität Zürich, Zurich, Switzerland
[65]Also at Stefan Meyer Institute for Subatomic Physics, Vienna, Austria
[66]Also at Laboratoire d'Annecy-le-Vieux de Physique des Particules, IN2P3-CNRS, Annecy-le-Vieux, France
[67]Also at Near East University, Research Center of Experimental Health Science, Mersin, Turkey
[68]Also at Konya Technical University, Konya, Turkey
[69]Also at Izmir Bakircay University, Izmir, Turkey
[70]Also at Adiyaman University, Adiyaman, Turkey
[71]Also at Bozok Universitetesi Rektörlügü, Yozgat, Turkey
[72]Also at Marmara University, Istanbul, Turkey
[73]Also at Milli Savunma University, Istanbul, Turkey
[74]Also at Kafkas University, Kars, Turkey
[75]Now at stanbul Okan University, Istanbul, Turkey
[76]Also at Hacettepe University, Ankara, Turkey
[77]Also at Istanbul University - Cerrahpasa, Faculty of Engineering, Istanbul, Turkey
[78]Also at Yildiz Technical University, Istanbul, Turkey
[79]Also at Vrije Universiteit Brussel, Brussel, Belgium
[80]Also at School of Physics and Astronomy, University of Southampton, Southampton, United Kingdom
[81]Also at IPPP Durham University, Durham, United Kingdom
[82]Also at Monash University, Faculty of Science, Clayton, Australia
[83]Also at Università di Torino, Torino, Italy
[84]Also at Bethel University, St. Paul, Minnesota, USA
[85]Also at Karamanoğlu Mehmetbey University, Karaman, Turkey
[86]Also at California Institute of Technology, Pasadena, California, USA
[87]Also at United States Naval Academy, Annapolis, Maryland, USA

[88]Also at Bingol University, Bingol, Turkey
[89]Also at Georgian Technical University, Tbilisi, Georgia
[90]Also at Sinop University, Sinop, Turkey
[91]Also at Erciyes University, Kayseri, Turkey
[92]Also at Horia Hulubei National Institute of Physics and Nuclear Engineering (IFIN-HH), Bucharest, Romania
[93]Now at an institute or an international laboratory covered by a cooperation agreement with CERN
[94]Also at Texas A&M University at Qatar, Doha, Qatar
[95]Also at Kyungpook National University, Daegu, Korea
[96]Also at another institute or international laboratory covered by a cooperation agreement with CERN
[97]Also at Universiteit Antwerpen, Antwerpen, Belgium
[98]Also at Yerevan Physics Institute, Yerevan, Armenia
[99]Also at Northeastern University, Boston, Massachusetts, USA
[100]Also at Imperial College, London, United Kingdom
[101]Also at Institute of Nuclear Physics of the Uzbekistan Academy of Sciences, Tashkent, Uzbekistan